Normalizing body weight with a dietary strategy mitigates obesity-accelerated pancreatic carcinogenesis in mice

Joanna Wirkus, Aya S. Ead, Irena Krga, Yige Wang, Matthew G. Pontifex, Michael Muller, David Vauzour, Karen E. Matsukuma, Guodong Zhang, Gerardo G. Mackenzie

PII: S0022-3166(25)00322-0

DOI: https://doi.org/10.1016/j.tjnut.2025.05.039

Reference: TJNUT 1039

To appear in: *The Journal of Nutrition*

Received Date: 3 March 2025

Revised Date: 5 May 2025

Accepted Date: 14 May 2025

Please cite this article as: J. Wirkus, A.S. Ead, I. Krga, Y. Wang, M.G. Pontifex, M. Muller, D. Vauzour, K.E. Matsukuma, G. Zhang, G.G. Mackenzie, Normalizing body weight with a dietary strategy mitigates obesity-accelerated pancreatic carcinogenesis in mice, *The Journal of Nutrition*, https://doi.org/10.1016/j.tjnut.2025.05.039.

Normalizing body weight with a dietary strategy mitigates obesity-accelerated pancreatic carcinogenesis in mice

Joanna Wirkus[1], Aya S. Ead[1], Irena Krga[1], Yige Wang[1], Matthew G. Pontifex[2], Michael Muller[2], David Vauzour[2], Karen E. Matsukuma[3,4], Guodong Zhang[1,4], Gerardo G. Mackenzie[1,4#]

[1]Department of Nutrition University of California, Davis, CA, USA; [2]Norwich Medical School, Biomedical Research Centre, University of East Anglia, Norwich NR4 7TJ, United Kingdom

[3]Department of Pathology and Laboratory Medicine, University of California, Davis Medical Center, Sacramento, CA.;[4]University of California, Davis Comprehensive Cancer Center, Sacramento, CA.

[#]Corresponding author: Gerardo G. Mackenzie, E-mail: ggmackenzie@ucdavis.edu

Abbreviations

AR, Androgen Receptor; Bcl-xL, B-cell lymphoma-extra large; CD, control diet; DIO, diet-induced obesity; ERK, Extracellular Signal-Regulated Kinase; GO, gene ontology; HIF1A, Hypoxia-Inducible Factor 1-alpha; KC mice, *LSL-Kras*$^{G12D/+}$*; p48*$^{Cre/+}$; NF-κB, Nuclear Factor kappa-light-chain-enhancer of activated B cells; PDAC, pancreatic ductal adenocarcinoma; SP1, Specificity Protein 1; STAT, Signal Transducer and Activator of Transcription

Conflict of Interest: Gerardo G. Mackenzie reports financial support was provided by National Institutes of Health. Gerardo G. Mackenzie reports financial support was provided by National Institute of Food and Agriculture. All other authors declare that they have no known competing financial interests or personal relationships that could have appeared to influence the work reported in this paper.

Running title: Diet Switch Prevents Obesity and Pancreatic Carcinogenesis

ABSTRACT

Background: Obesity is a modifiable risk factor for pancreatic cancer, but the impact of dietary changes leading to weight loss in pancreatic carcinogenesis remains unknown.

Objective: To determine the effects of weight normalization via dietary switch on pancreatic carcinogenesis and associated mechanisms.

Methods: Five-week-old male and female *LSL-Kras$^{G12D/+}$; p48$^{Cre/+}$* (KC) mice (8-12/diet group/sex) were fed a high-fat, diet-induced obesity diet (DIO; 60% kcal from fat) or a low-fat, control diet (CD; 11% kcal from fat) for 21 weeks. A subset of mice was fed the DIO for 8 weeks, then switched to CD for 13 additional weeks (DIO→CD). Cancer incidence was evaluated by histology. Lipidomics and RNAseq followed by bioinformatic analysis identified potential mechanisms. The gut microbiome was characterized using 16s rRNA amplicon sequencing. Data were analyzed using one-way analysis of variance.

Results: After 21 weeks, DIO-fed mice had 1.7-fold higher body weight gain, and 60% increase ($p<0.05$ DIO vs. CD) in pancreatic acinar-to-ductal metaplasia, compared to the other 2 groups. None of the 21 mice fed a CD developed cancer, while 2 out of 21 DIO-fed male mice did. Switching from a DIO to a CD normalized body weight and composition to CD levels, slowed acinar-to-ductal metaplasia and prevented cancer incidence, with no mice developing cancer. Mechanistically, DIO affected gene expression related to cellular metabolism, pancreatic secretions, immune function, and cell-signaling, while CD and DIO→CD had similar global gene expression. Moreover, DIO increased epoxy metabolites of linoleic acid, which were mitigated by the dietary switch. Finally, compared to a CD, DIO altered the gut microbiome and switching from a DIO to a CD restored the gut microbiome profile to resemble that of CD-fed mice.

Conclusions: Body weight normalization slowed obesity-accelerated pancreatic carcinogenesis, in part, by affecting inflammatory and cell signaling pathways, reducing epoxy metabolites, and modulating the gut microbiome.

Keywords: high-fat diet, pancreatic carcinogenesis, obesity, pancreatic cancer, gut microbiome

1. Introduction

Pancreatic ductal adenocarcinoma (PDAC) is a life-threatening and costly disease with rising incidence (1). It significantly lowers the quality of life, kills 87% of patients within five years, and is projected to cost $3.8 billion in healthcare expenditures by 2030 (2, 3). Therefore, efforts to prevent this deadly disease are urgently needed, with dietary strategies representing a critical approach.

Obesity poses a significant public health problem due to its association with many chronic diseases and 13 types of cancer, including PDAC (4, 5). Indeed, excess body fatness is a major modifiable risk factor for developing PDAC, increasing its risk by around 50% and leading to earlier diagnosis and poorer prognosis (6). Over the past decade, multiple preclinical studies have investigated the impact of high-fat, high-calorie diets on pancreatic cancer development, clearly documenting that diet-induced obesity accelerates pancreatic carcinogenesis, including at early stages (7-10). Recently, we demonstrated that feeding a high fat diet for 8 weeks results in increased body weight and accelerates early stages of pancreatic carcinogenesis in male KC mice (9). Although obesity can be caused, in part, by increased dietary fat and calorie intake, the underlying mechanisms that lead to the development of obesity-associated PDAC are complex and still incompletely understood. In addition, it remains unclear whether weight loss through dietary changes could alter the course of pancreatic carcinogenesis.

Notably, the role of weight loss in cancer prevention is a significant area of research. Studies in humans indicate that bariatric surgery can reduce the risk of developing pancreatic cancer (11, 12). Furthermore, caloric restriction has also been shown to decrease tumor burden in a genetically obese mouse model of pancreatic cancer (13). Among the various strategies, dietary changes are the least invasive and risky for managing high body fat. In mice, transitioning from a high-fat, obesity-inducing diet to a low-fat control diet has been explored as a method to reduce the risk of various cancers, such as breast, endometrial, and colon cancer (14-16).

However, despite the evidence linking high fat diet, obesity, and acceleration of early stage carcinogenesis (8, 9, 17), the role of reducing body weight with dietary changes, in preventing pancreatic cancer, and the associated mechanisms, remains unclear.

Therefore, in this study, we assessed how changes in dietary fat quantity, leading to weight normalization, affect pancreatic carcinogenesis in a clinically relevant mouse model of pancreatic cancer [*LSL-Kras*$^{G12D/+}$*; p48*$^{Cre/+}$ (KC)]. The KC mice conditionally express the endogenous mutant Kras allele in pancreatic cells, contain ductal lesions that mirror human pancreatic intraneoplasias (PanINs), closely mimicking the pathophysiological and cellular features observed in human PDAC development (18, 19). Moreover, as the KC mice age, the acinar parenchyma is replaced by stromal or desmoplastic fibroblasts and inflammatory cells, which is highly reminiscent of that seen in human pancreatic cancers (18, 19). For this purpose, we fed five-week-old KC mice one of three dietary treatments. Two groups were fed either a high-fat or a low-fat diet until six months of age. A third group was initially fed a high-fat diet for eight weeks until three months of age, then switched to a low-fat control diet for an additional 13 weeks, until six months of age. We observed that switching KC mice from a high-fat diet to a low-fat diet slowed pancreatic acinar-to-ductal metaplasia and prevented cancer incidence. This effect was partly due to the modulating of genes involved in cellular metabolism, immune function, and cell signaling, reducing epoxy metabolites of linoleic acid, and restoring the gut microbiome composition.

2. Materials and Methods

2.1. Materials

Sigma REDExtract-N-AMP Tissue PCR Kit for DNA extraction (Cat# XNAT-10RXN) and Calcium phosphate dibasic (Cat# C7263-100G) for diets were obtained from Sigma Aldrich (St. Louis, MO). PCR amplification was conducted using Quick-Load® Taq 2X Master Mix (Cat#

M0271L) from New England Biolabs® Inc. (Ipswich, MA). Agarose (Cat# BP164-25), Biotium GelRed Nucleic Acid Gel Stain 10,000X in DMSO (Cat# NC9524151), primers, phosphatase inhibitor (Cat# A32957), RNAlater RNA Stabilization Solution (Cat# AM7021), cellulose (Cat# ICN90045305), and alphacel non-nutritive bulk (MP Biomedicals,Santa Ana, CA) were purchased from Fisher Scientific (Waltham, MA). American Institute of Nutrition (AIN93G) diet (Cat# D110700), casein (Cat# 400600), L-cysteine (Cat# 401340), maltodextrin (Cat# 402850), lard (Cat# 402400), soybean oil (stabilized with 0.02% w/v Tert-Butylhydroquinone (tBHQ) (Cat# 404360), and tBHQ (Cat# 404455), were procured from Dyets, Inc. Mineral Mix (Cat# TD.94046) and Vitamin Mix (Cat# CA.40060.PWD) were acquired from Envigo/Teklad Custom Diet (Indianapolis, IN). Cornstarch was obtained from Tate & Lyle (Decatur, IL), sucrose from California and Hawaiian Sugar Company (Crockett, CA), and Archer Daniels Midland dextrose were purchased from Restaurant Depot (Sacramento, CA).

Western blot primary antibodies, including phospho-p44/42 MAPK (Erk1/2) $^{(Thr202/Tyr204)}$ (Cat# 4370), p44/p42 MAPK (Erk1/2) (Cat# 9102), phospho-Stat3$^{(Try705)}$ (Cat# 9145), and Stat3 (Cat# 30835), vinculin (Cat# 13901), and Bcl-xL (Cat# 2764), along with the secondary anti-rabbit antibody (Cat# 7074) were purchased from Cell Signaling Technology (Danvers, MA). Western blot supplies: EveryBlot blocking buffer (Cat# 12010020), 2x Laemmli sample buffer (Cat# 1610737), Protein Assay Dye Reagent Concentrate (Cat# 50000060), polyvinylidene diflouride (PVDF) membranes (Cat# 1620184), Precision Plus Protein™ Dual Xtra Prestained Protein Standards (Cat# 1610397) came from Bio-rad, Hercules, CA. IGEPAL CA630 (Cat# I3021) and protease inhibitor (Cat# 11836170001) were purchased from Millipore-Sigma. ECL reagent (Cat# 20-300B) was purchased from Prometheus Protein Biology Products, Genesee Scientific, (El Cajon CA).

2.2. Experimental animal design, diets, and sample collection

Mice were housed within an Association for Assessment and Accreditation of Laboratory Animal Care, International (AAALAC)-accredited animal facility located at the University of California (UC), Davis. The study protocols (#22057) were approved by the UC Davis Institutional Animal Care and Use Committee (IACUC) to ensure adherence to ethical regulations. Throughout the study's duration, mice were housed in a controlled environment, maintained at temperatures ranging from 22-24°C, with a relative humidity of 40-60%, and a 12-h light-dark cycle, and had *ad libitum* access to food and water. Daily health status monitoring was conducted with humane endpoints in place.

KC mice, in the C57BL/6J background, were procured via in-house breeding, involving the crossing of $p48^{Cre/+}$ positive mice with $LSL\text{-}Kras^{G12D/+}; p48^{Cre/+}$ (KC) positive mice. KC mice originated from the National Cancer Institute mouse repository and were established following procedures outlined in Hingorani et al (20). Offspring were genotyped using PCR between 7 and 12 d old (primers: KRAS Sense 5' CCT TTA CAA GCG CAC GCA GAG 3' KRAS Antisense 5' AGC TAG CCA CCA TGG CTT GAG TAA GTC TGC A 3' P48-Cre Forward 5' ACC GTC AGT ACG TGA GAT ATC TT 3' P48-Cre Reverse 5' ACC TGA AGA TGT TCG CGA TTA TCT 3'). Only animals carrying both mutations [$LSL\text{-}Kras^{G12D/+}; p48^{Cre/+}$] were enrolled in the feeding trial.

At three weeks of age, KC mice were weaned, co-housed, and fed an AIN93G diet (Cat # 110700; Dyets Inc., Bethlehem, PA) for 2 weeks until enrolled in the studies. At 5 weeks of age, KC mice (8-10 males and 9-12 females per diet group) were singly housed and randomized to a dietary treatment group using a random number generator. Once groups were half full, mice were assigned to a dietary treatment group by body weight to create groups with roughly equal enrollment body weight to align with the essential 10 Animal Research: Reporting of In Vivo Experiments (ARRIVE) 2.0 guidelines on randomization (21). KC mice were enrolled into one of three dietary treatment groups and fed a: [1] low-fat (11% kcal from fat) control diet (CD) modeled after the AIN93M diet, [2] high-fat Diet-Induced Obesity diet (DIO), or [3] a DIO switch to a CD (DIO→CD). Diet recipes are included in **Supplemental Table 1**. Fatty acids composition for the

CD and DIO, assessed using gas chromatography, have been previously described (10). Of note, both diets (CD and DIO) met and exceeded the nutrient requirements set forth by the National Research Council's Nutrient Requirements of the Mouse (22), although they presented differences in the vitamins' content, to address possible nutrient losses during manufacturing.

The DIO→CD mice were fed the DIO for 8 weeks until 3 months of age, then switched to the CD for an additional 13 weeks, until 6 months of age. The purified diets were fed for 21 weeks and the feeding study ended when the mice were 6 months of age (**Figure 1A**).

Food intake was recorded weekly. Grams of food consumed per day was multiplied by the caloric density of the food to determine caloric intake (3.55 kcal/g for the CD and 5.10 kcal/g for the DIO). Fresh food was provided every 2-3 days.

Body weight was measured once per week (Mettler Toledo scale) and body composition (fat and lean mass) was measured using an EchoMRI-100H (EchoMRI LLC, Houston, TX) at 3 and 6 months of age.

At the endpoint, KC mice were euthanized by CO_2 asphyxiation. Pancreas, cecum, and various adipose depots (bilateral inguinal fat pads, mesenteric adipose, gonadal or epididymal fat, and the interscapular brown adipose tissue) were collected and weighed. The pancreas was submerged in protease and phosphatase inhibitors prior to its portions being flash frozen in liquid nitrogen, collected for histology, or for RNA isolation.

2.3. Nonfasting capillary blood glucose levels

Glucose levels were measured using a glucometer (Easy Plus II 1652) between 12-2 pm prior to experimental diet initiation (at 5 weeks of age) and at the end of dietary intervention.

2.4. Hemoglobin A1c levels

Prior to necropsy, blood (~20 µl) was collected into a microvette EDTA plasma tube (Cat# 16.444.100, Kent Scientific Corporation, Torrington, CT) using a submandibular cheek punch

with a 5.5 mm lancet. Hemoglobin A1c was assessed using the Mouse Hemoglobin A1c Assay Kit (Cat #80310) from Crystal Chem (Elk Grove Village, IL) according to the manufacturer's instructions.

2.5. Histological analysis

For histology, the pancreas was processed with 10% w/v formalin fixation at 4°C overnight, ethanol dehydration, and embedding in paraffin blocks. Four-micrometer-thick sections were routinely prepared, and subsequently stained utilizing hematoxylin and eosin (H&E) and Masson's Trichrome at the UC Davis Pathology Biorepository.

In the H&E stained slides, the area of acinar-to-ductal metaplasia (ADM) was assessed as percentage of ADM over the whole pancreas section, by five investigators blinded to the study conditions using an Olympus BX46 microscope (Olympus Corporation, Shinjuku City, Tokyo, Japan) at 4x and 10x. The morphological grading of PanINs (low-grade or high-grade) was performed based on the degree of cytoarchitecture and nuclear heterogeneity, as previously described (18, 23, 24). Presence or absence of cancer, as well as the PanIN grading, was blindly assessed by the pathologist on our team (K.M). One slide per sample was assessed. Furthermore, the Masson's Trichrome stained slides were similarly microscopically evaluated to assess percentage of fibrotic tissue. Fibrosis data from three investigators blinded to the study conditions were subsequently averaged after the exclusion of discordant values.

2.6. Western blot analysis

Pancreatic tissue homogenates were prepared using sucrose lysis buffer [1M Tris, pH 7.5, 1M sucrose, 1mM EDTA, 1mM EGTA, phosphatase inhibitor, protease inhibitor complex, IGEPAL] and BeadMill24 tissue homogenizer (Thermo Fisher Scientific Inc., Piscataway, NJ). Following the centrifugation at 6000 RPM for 10 min at 4°C, supernatants were collected, and protein concentration was determined using the Bradford assay (25). Aliquots of total

193 homogenates containing 15 µg of protein, denatured in Laemmli sample buffer, were separated
194 by a reducing 12% (w/v) polyacrylamide gel electrophoresis at 180 V, and electroblotted to PVDF
195 membranes. Colored molecular weight standards were run simultaneously. Membranes were
196 blocked for 5 min with EveryBlot blocking buffer (Bio-Rad, Hercules, CA), and subsequently
197 incubated in the presence of the corresponding primary antibody (1:1000 dilution) overnight at
198 4°C. After incubation for 60 min at room temperature in the presence of a HRP conjugated
199 secondary antibody (1:2000 dilution) the conjugates were visualized using enhanced
200 chemiluminescence. Images were taken using Bio-Rad ChemiDoc Imager (Bio-Rad, Hercules,
201 CA). The densitometric analysis was performed using ImageJ Fiji software (National Institutes of
202 Health, Bethesda, MD).
203
204 *2.7 RNA extraction and RNA-sequencing analysis*

205 Pancreatic tissues were stabilized in RNAlater (Cat# AM7021, ThermoFisher Scientific,
206 Waltham, MA). Total RNA was extracted from the pancreas of three female mice per
207 experimental group (CD, DIO, DIO→CD) using the RNeasy mini kit (Cat# 74104, QIAGEN,
208 Hilden, Germany), and residual amounts of DNA were removed using an on-column RNase-Free
209 DNase Set (Cat# 79254 QIAGEN) according to the manufacturer's instructions. RNA quality
210 measured by A260/A280 ratios of 2 or higher were confirmed using a NanoDrop One
211 Spectrophotometer (ND-ONE-W) (Thermo Scientific, Waltham, MA). Library preparation and
212 RNA-sequencing were performed by Novogene Co., LTD (Beijing, China). In brief, mRNA was
213 enriched using oligo(dT) beads, and rRNA was removed using the Ribo-Zero kit. The mRNA was
214 fragmented, and cDNA was synthesized by using mRNA template and random hexamers primer,
215 after which a second-strand synthesis buffer (Illumina), dNTPs, RNase H and DNA polymerase
216 I were added for the second-strand synthesis, followed by adaptor ligation and size selection.
217 The library was sequenced by the Illumina Novaseq platform. Paired sequence reads were

aligned to mm10 genome using HISAT2 tool, and then counted and normalized using the feature Counts accessed through Galaxy platform. Differential gene expression in DIO vs. CD and DIO→CD vs. DIO groups were identified using DESeq2 tool in Galaxy. All genes with Benjamini-Hochberg corrected p-value < 0.05 and ±1.4-fold change, were considered differentially expressed. Volcano plots of gene expression profiles were created using VolcaNoseR.

2.8 Bioinformatic analysis

To compare gene expression profiles, principal Component Analysis (PCA) plot and hierarchical clustering heatmaps with the Euclidean distance and the ward's clustering were created using MetaboAnalyst (https://www.metaboanalyst.ca; (26)).

Gene expression data from DIO vs. CD and DIO→CD vs. DIO comparisons were used to perform biological process and pathway enrichment analyses using Genetrail 3.2 with theaccess to Gene Ontology (GO) and Kyoto Encyclopedia of Genes and Genomes (KEGG). Significant enriched/depleted processes and pathways were obtained by Kolmogorov-Smirnov test (GSEA) with Benjamini-Yekutieli FDR adjustment. GO enrichment bubble plot was generated by SRplot (27), pathway enrichment histograms using Microsoft Excel and Venn diagrams by Venny 2.1.0 (https://bioinfogp.cnb.csic.es/tools/venny/).

Potential transcription factors whose activity could be modulated by the experimental diets were identified using enrichment analysis with Bonferroni correction in Metascape (28). TRRUST (29) database was used to search for the potential transcription factors. Finally, the association of identified differentially expressed genes with human diseases was analyzed using the Comparative Toxicogenomics Database (https://ctdbase.org/) (30). Significantly enriched diseases were calculated by the hypergeometric distribution, adjusted by Bonferroni method.

2.9 Liquid Chromatography-Tandem Mass Spectrometry (LC-MS/MS)-based lipidomic analysis

Mouse pancreases tissue (15-35 mg) was mixed with 20μL isotope-labeled surrogate standard solution and 10 μL antioxidant solution (0.2 mg/mL butylated hydroxytoluene and 0.2 mg/mL triphenylphosphine in methanol), followed by the addition of methanol [400 μL containing 0.1% acetic acid and 0.1% butylated hydroxytoluene (BHT)], then stored at -80 °C for 30 min. After freezing, samples were homogenized using a homogenizer, stored at -80°C overnight, and then centrifuged to collect the supernatant. The supernatants were diluted with 1.5 mL of Millipore water, then extracted using solid phase extraction (SPE) columns. Briefly, Waters Oasis HLB columns (60 mg, 3cc cartridges; Waters, Milford, MA) were pre-conditioned by washing twice with 3 mL ethyl acetate, twice with 3 mL methanol, and twice with 3 mL SPE washing buffer (95:5 water/methanol with 0.1% acetic acid). The sample was then loaded onto the column and washed twice with 3 mL washing buffer. The SPE filter was dried under vacuum for 20 min. Oxylipins were eluted with 0.5 mL methanol and 1.5 mL ethyl acetate into 2-mL collection tubes containing 10 μL trap solution (30% glycerol in methanol). Samples were dried by vacuum centrifugation and reconstituted in 50 μL methanol containing 200 nM 1-cyclohexyl ureido, 3-dodecanoic acid (CUDA) as a surrogate recovery standard. The reconstituted samples were filtered using Ultrafree-MC VV Centrifugal Filter (0.1 μm; EMD Millipore, Bedford, MA, USA) for LC-MS/MS analysis.

The LC-MS/MS analysis was performed on an Agilent 1200SL HPLC system coupled to a 4000 QTRAP MS/MS, as described in our previous reports (31). Peaks were identified based on retention time and specific multiple reaction monitoring (MRM) transitions of the lipid metabolite standards. The concentrations of the lipid metabolites were calculated using calibration curves with standards.

2.10 Fecal sample collection and microbiome analysis

Up to 4 days prior to necropsy, fecal samples were collected into a cryogenic tube, flash frozen in liquid nitrogen, and stored at -80°C until analysis. Genomic DNA was extracted using a commercially available kit (Qiagen QIAamp PowerFecal Pro DNA Kit, Cat. 51804) and following manufacturer's instructions. DNA concentrations of each sample were evaluated using Qubit® dsDNA High Sensitivity Assay Kit (Cat. Q32851) with Qubit® 4.0 Fluorometer, following manufacturer's instructions. Quality assessment was performed by agarose gel electrophoresis to detect DNA integrity, purity, fragment size, and concentration. The 16S rRNA amplicon sequencing of the V3-V4 hypervariable region was performed with an Illumina NovaSeq 6000 PE250. Sequence analyses were performed by Uparse software (Uparse v7.0.1001) (32), using all the effective tags. Sequences with ≥97% similarity were assigned to the same OTUs. Representative sequence for each OTU was screened for further annotation. For each representative sequence, Mothur software was performed against the SSUrRNA database of SILVA Database (33). OTUs abundance data were normalized using a standard of sequence number corresponding to the sample with the least sequences.

The α- and β-diversity were assessed by using standard metrics (e.g. Simpson and Shannon H diversity index) and Bray-Curtis Principal Coordinates of Analysis (PCoA), respectively. Statistical significance was determined by Kruskal–Wallis or Permutational Multivariate Analysis of Variance (PERMANOVA). Comparisons at the Phylum and Genus level were made using classical univariate analysis using Kruskal–Wallis combined with a false discovery rate (FDR) approach used to correct for multiple testing. Finally, LEfSe (Linear discriminant analysis Effect Size) was also employed to determine the features most likely to explain differences between classes.

2.11 Short chain fatty acids

Cecal content was collected at necropsy, snap frozen in liquid nitrogen, and stored at -80°C until further analysis. The West Coast Metabolomics Center (Davis, CA) analyzed short

chain fatty acids (acetic acid, butyric acid, formic acid, isovaleric acid, propionic acid, and valeric acid). Briefly, cecal content (10 mg) was extracted using a biphasic method. The extraction involved adding 0.5 mL of water with internal standards, 0.1 mL of concentrated HCl, and 1 mL of Methyl Tert-Butyl Ether. The samples were shaken for 30 min at room temperature and then centrifuged for 2 min at 14,000 rcf. From the organic phase, 100 µL was aliquoted into a glass crimp vial containing 25 µL of N-tert-Butyldimethylsilyl-N-methyltrifluoroacetamide. The vials were crimp-capped and shaken at 80°C for 30 min to complete the derivatization process.

After derivatization, the vials were placed in a gas chromatography (GC) sampler for analysis. A 1 µL aliquot of the derivatized sample was injected using a split method at an inlet temperature of 250°C. The GC run was conducted with a constant helium flow of 1.2 mL/min. The oven temperature program started at 50°C for 0.5 min, ramped to 70°C at 5°C/min, held for 3.5 min, then ramped to 120°C at 10°C/min, and finally ramped to 290°C at 35°C/min, holding for 3 min, resulting in a total run time of 20.857 min. The transfer line was set to 290°C, and the electron ionization source was set to 250°C.

Mass spectrometry (MS) parameters were set to collect data from 85 m/z to 5 m/z at an acquisition rate of 17 spectra/s. A 6-point calibration curve with internal standards was injected alongside the samples for absolute quantification. Additionally, a pooled sample was used as a quality control measure and injected every ten samples. Data processing and target peak identification were performed using Mass Hunter Quant, with normalization to the amount of sample injected.

2.12 Statistical analysis

2.12.1 Sample size determination: We aimed to include a cohort of 20 KC mice per diet group, with 10 males and 10 females per diet group. Based on a prior study (8), we expected that the difference between the highest and lowest mean percentages of acinar-to-ductal metaplasia among the 3 groups at month 6 will be at least 1.5 SD. The total sample of 60 mice

at month 6 (= 20 mice x 3 groups) will have 99% power to detect the difference of 1.5 SD between the highest and lowest means using an F test with a 0.05 significance level. We will also have at least 83% power to detect the difference of 1.5 SD within each sex subgroup. Due to attrition, the DIO→CD group had only 8 male mice by the endpoint.

2.12.2 Data analysis: Data are shown as mean ± standard deviation (SD). Male and female mice were analyzed separately using a one-way ANOVA to determine the difference between the means of the groups. In some instances, data for both male and female mice was analyzed together, if a two-way ANOVA determined no differences between male and female mice. A post hoc Tukey test was used to address multiple comparisons. Weight data was analyzed using a mixed effects analysis. Cancer incidence was analyzed using a Fisher's exact test. Analysis was done using GraphPad Prism software 10.0.0 for Windows (Graph-Pad Software Boston, Massachusetts USA, www.graphpad.com). A p value of < 0.05 was considered statistically significant.

2.13 Data availability: The accession number for the RNA-Seq data reported in this study is NCBI Gene Expression Omnibus: GSE293790. The accession number for the microbiome data is under Bioproject number: PRJNA1245375

3. Results

3.1 Dietary switch from a DIO to a CD normalizes diet-induced weight gain and body composition in male and female KC mice.

To determine the effects of CD, DIO, and diet switch from DIO to CD on body weight gain, mice were weighed weekly over the 21-week feeding period. All mice gained weight, but KC mice on the DIO gained significantly more than those on the CD. After 8 weeks, DIO-fed

male and female KC mice weighed significantly more than CD-fed mice ($p < 0.01$ for both; **Fig. 1B**).

At the endpoint, the average body weight of the dietary switch group was similar to the CD group (**Fig. 1C**). While the DIO-fed male KC mice weighed 48 ± 6 g, the CD and DIO→CD-fed males weighed significantly less (35 ± 6 g, and 36 ± 4 g, respectively). A similar trend was observed in females (**Fig. 1C**).

Body composition was assessed at 3 months of age (before diet change) and at 6 months of age. After 8 weeks on their respective diet, DIO-fed mice had significantly more body fat and less lean mass compared to CD-fed mice (**Fig. 1D**). The body composition changes induced by DIO were even more pronounced at 6 months of age. Switching from the DIO to the CD normalized body composition by the end of the study (**Fig. 1E**).

Changes in body composition were associated with weight changes of multiple fat depots. While DIO-fed mice had higher weights of subcutaneous, mesenteric, as well as epididymal/gonadal fat, switching from DIO to CD normalized the weight of these adipose depots to CD levels in both male and female KC mice (**Supplemental Figure 1**). No significant differences among the three groups were observed when comparing the average weight of the interscapular brown adipose tissue (BAT) depot (**Supplemental Figure 1**).

We also assessed calorie intake throughout the 21-week feeding study. During the first 8 weeks of feeding, the CD fed KC mice ate 13.0 ± 1.1 kcal/day and the DIO fed KC mice ate 14.4 ± 2.0 kcal/day ($p < 0.001$; **Fig. 2A**). During the last 3 months of the study, the CD-fed KC mice continued to consume fewer calories on average (12.7 ± 0.4 kcal/day) than the DIO-fed (14.7 ± 0.6 kcal/day) KC mice ($p < 0.001$; **Fig. 2B**). After the dietary switch, the average daily calorie intake of the KC mice in the group that changed from the DIO to the CD was similar to that of the mice that remained in the CD (DIO→CD 13.0 ± 0.6 kcal/day) (**Fig. 2B**).

Then, we measured the effect of the dietary changes on glucose and hemoglobin A1c levels as a result of the dietary interventions. Blood glucose levels at baseline (data not shown)

and at endpoint, were all within normal limits for a nonfasting capillary glucose measurement and similar among the CD, DIO and DIO→CD groups (**Fig. 2C**). Similarly, with around 4% hemoglobin A1c for all groups, none of the mice displayed evidence of clinically significant hyperglycemia that would indicate prediabetes or diabetes mellitus (**Fig. 2D**).

3.2 Body weight normalization mitigates pancreatic carcinogenesis and reduces cancer incidence in KC mice.

At necropsy, we weighed and collected the pancreata of KC mice in the three dietary treatment groups. Feeding a DIO to KC mice for 21 weeks resulted in a higher average pancreas weight (0.72 ± 0.22 g) compared to CD-fed mice (0.46 ± 0.10 g). The difference between DIO and CD-fed KC mouse pancreas weight remained significant when analyzed by sex (male CD 0.43 ± 0.06 g; male DIO 0.74 ± 0.28 g; female CD 0.48 ± 0.10 g; female DIO 0.71 ± 0.17 g) ($p < 0.05$; **Fig. 3A**). Switching from a high-fat to a low-fat diet in female KC mice (DIO→CD) resulted in significantly lower pancreas weight (0.50 ± 0.20 g) compared to DIO-fed mice ($p < 0.05$; **Fig. 3A**). Similar effects were observed in males.

We then assessed acinar-to-ductal metaplasia (ADM), a precursor to pancreatic cancer, by H&E histology. DIO-fed KC mice had the highest ADM (80 ± 14%), which was significant compared to CD-fed mice (50 ± 23%) ($p < 0.001$; **Fig. 3B**). Dietary changes ameliorated pancreatic transformation (DIO→CD = 55 ± 21%; $p < 0.05$). Indeed, ADM was lower in the DIO→CD group compared to DIO-fed mice (**Fig. 3B**). When separated by sex, DIO-fed male KC mice had higher ADM levels in mice compared to CD group (83 ± 15% vs. 47 ± 22%, $p < 0.01$; **Fig. 3B**). The dietary switch group had ADM levels similar to CD-fed male KC mice ($p > 0.05$; **Fig. 3B**). Similar effects of diet on pancreatic ADM were observed in female KC mice (**Fig. 3B**).

Next, we assessed pancreatic fibrosis using Masson's trichrome staining. DIO-fed mice had higher fibrosis (83 ± 10%) compared to CD-fed mice (54 ± 19%) ($p < 0.01$; **Fig. 3B**). This pattern persisted when analyzed by sex (male CD: 53 ± 20%, male DIO: 86 ± 5%; female CD:

54 ± 20%, female DIO: 82 ± 13%) ($p < 0.05$; **Fig. 3B**). The DIO→CD fed mice had fibrosis levels significantly lower than the DIO group (**Fig. 3B**).

Moreover, we observed a positive significant association between body weight and ADM in both males and females. While DIO group samples cluster toward top right direction, the DIO→CD fed mice clustered closer to the CD group (**Figure 3C)**. Similar positive correlations are observed between fat mass and ADM (**Supplemental Figure 2**). These correlations suggest that the increase in ADM in the DIO group might be due to higher body weight and/or fat mass in these mice.

Next, we assessed whether the DIO accelerated early pancreatic neoplasia. Histological evaluation of pancreatic tissue sections revealed that after 21 weeks, DIO displayed significantly more cases that presented high-grade PanINs, compared to CD and DIO→CD groups in male mice. In contrast, no differences in females were observed among the groups (**Figure 3D).**

Finally, we examined cancer incidence. While no cancer was observed in females, two out of nine (22%) male KC mice in the DIO group developed pancreatic cancer. No cancer incidence was observed in male and female mice fed the CD or those mice that switched from the DIO to the CD (**Fig. 3E**).

3.3 Normalizing body weight reverses pancreatic gene expression induced by obesity

To evaluate potential molecular mechanisms involved in DIO-accelerated pancreatic carcinogenesis, we initially assessed the global expression of genes in the pancreas of KC mice fed a DIO or CD for 21 weeks. DIO significantly altered pancreatic gene expression, with 2,167 differentially expressed protein coding genes in DIO-fed mice compared to CD mice (**Fig. 4A**). Gene ontology (GO) and pathway enrichment analyses revealed that these differentially expressed genes are involved in pancreatic secretion (**Supplemental Table 2)**, inflammation, immune function, metabolism, and cancer-related pathways (**Fig. 4B, and Supplemental Figure 3A**) and are associated with neoplasms and metabolic diseases (**Supplemental Table 3**). Of

note, key transcription factors possibly mediating the observed nutrigenomic effects included NF-κB, SP1, STAT1, and STAT3 (**Supplemental Table 4**).

Switching from DIO to CD reversed many of these protein coding gene expression changes, with 1,017 differentially expressed genes identified (**Fig. 4C**). GO analysis showed that the diet switch affected immune system regulation, cell motility, and cytokine production (**Supplemental Figure 3B**) and pathway analyses indicated involvement in inflammation, immune function, and metabolism (**Fig. 4B**). These modulated genes were linked with neoplasms and metabolic disorders (**Supplemental Table 5**). Key transcription factors possibly underlying the genomic effects of a dietary switch included SP1, NF-κB, AR, and HIF1A (**Supplemental Table 6**)

Comparative analysis of gene expression profiles using principal component analysis showed that the DIO and dietary switch groups had distinct profiles, with the switch group resembling the CD group (**Fig. 5A**). Moreover, genes significantly modulated following both DIO and DIO→CD showed opposing direction of gene expression (**Fig. 5B**). These data suggest that dietary changes can reverse DIO-induced gene expression alterations. Common pathways inversely affected by the DIO and dietary switch included those related to pancreatic secretion (**Supplemental Table 2)**, inflammation and immune function (**Fig. 5C**), with NF-κB, SP1, and STAT3 as potential key regulators (**Supplemental Table 7**).

To validate some of these findings, we conducted Western blot analyses of key regulators. For example, the STAT3 pathway implicated in the pathway related to inflammation was upregulated in the pancreas of mice fed the DIO, while their levels were ameliorated in the dietary switch group (**Fig. 5D**). Similarly, phosphorylated ERK levels in the pancreas of male mice were upregulated by the DIO, while DIO→CD mitigated these effects **(Fig. 5E)**. No effects were observed on Bcl-xL levels (**Supplemental Figure 4**).

3.4 Body weight normalization mitigates the increased pancreatic levels of epoxide derivatives of linoleic acid triggered by diet-induced obesity.

The RNAseq data analysis suggested that the mRNA levels of the enzyme 5-lipoxygenase (5-LOX), a key enzyme in eicosanoid metabolism, were 2.34-fold higher in DIO, compared to CD group, and it was partially reduced in the DIO→CD group (**Supplemental Figure 5**). Given that eicosanoids are important regulators of inflammation, immune response, and tumorigenesis (34, 35), we next conducted LC-MS/MS–based lipidomics to compare the profiles of eicosanoid metabolites in the pancreatic tissues of CD-, DIO- and DIO→CD-fed mice (**Fig. 6A)**. We detected 42 eicosanoids in pancreatic tissues (some eicosanoids were below the detection limit of our LC-MS/MS method). The most significant DIO-related changes were observed in the ω-6-series metabolites derived from linoleic acid (LA, 18:2ω-6). Notably, altered LA metabolites included 9,10- and 12,13-epoxy-octadecenoic acids (EpOMEs), produced by cytochrome P450 (CYP) monooxygenases, as well as 9-hydroxy-octadecadienoic acid (9-HODE) and 9-oxo-octadecadienoic acid (9-oxo-ODE), which are generated by enzymes such as 5-LOX (**Fig. 6B**).

In addition to the LA-derived metabolites, DIO-fed mice exhibited elevated levels of ω-3-series metabolites derived from α-linolenic acid (ALA, 18:3ω-3), including 9,10-, 12,13-, and 15,16-epoxyoctadecadienoic acids (EpODEs) and 9-hydroxy-octadecatrienoic acid (9-HOTrE) compared to the CD group. All the DIO-induced changes in these metabolites were mitigated following the dietary switch (**Fig. 6B-C**). However, the levels of these ω-3-series metabolites are relatively low (**Fig. 6C**).

3.5 Normalizing body weight mitigates obesity-associated gastrointestinal microbiome composition alterations.

Finally, given the role of the gut microbiome in pancreatic cancer (36), we evaluated the effect of body weight normalization on the gut microbiome during pancreatic carcinogenesis.

Compared to CD, DIO-fed mice had higher α-diversity, as measured by Simpson and Shannon index (**Fig. 7A**). Lowering dietary fat quantity reversed α-diversity back to CD levels, with the dietary switch group having an α-diversity similar to the CD group (**Fig. 7A**).

We next performed a Bray-Curtis principal component of analysis (PCoA) to define the similarity of species diversity among groups on operational taxonomic unit (OTU) level (**Fig. 7B**). There was a significant impact of dietary treatment on microbial beta-diversity, with the dietary switch group clustering closer to CD group (**Fig. 7B**).

At the phylum level, Firmicutes and Bacteroidota dominated the GI microbiome of KC mice in all diet groups (**Fig. 7C**). The dietary switch group had increased relative abundance of the phylum Bacteroidota and decreased relative abundance of Firmicutes compared to continuously CD- and DIO-fed mice. Relative abundance levels of Proteobacteria and Desulfobacterota were lower in the DIO-fed mice compared to CD. Desulfobacterota in the DIO→CD group was similar to the CD group (**Fig. 7C**).

Feeding a DIO resulted in a similar abundance of *Lactobacillus* as CD and increased the abundance of genera *Bacteroides*, *Erysipelatoclostridium* and *Enterococcus*, while decreasing the abundance of *Muribaculaceae* family and genera *Faecalibaculum* and *Dubosiella*. The dietary switch group had *a higher abundance of Bacteroides* than either the DIO or CD, while *Lactobacillus* abundance was reduced compared to the other groups (**Fig. 7**). DIO → CD dietary switch mitigated the DIO-induced changes in *Erysipelatoclostridium*, *Enterococcus*, *Faecalibaculum, Dubosiella and Muribaculaceae. It also* significantly reduced the abundances of DIO-induced increases in genera *Blautia*, *Roseburia* (family *Lachnospiraceae*), *Oscillibacter*, *Intestinimonas*, and *Colidextribacter* (family *Oscillospiraceae*), and ultimately class *Clostridia*, bringing them to levels similar to those observed in the CD-fed mice (**Fig. 8**).

In addition to characterizing the levels of relative microbial abundance, we measured microbial metabolites, short chain fatty acids (SCFA), in the cecal contents of male and female KC mice in the CD, DIO and DIO→CD groups. There were no significant differences in the levels

499 of acetic acid, butyric acid, formic acid, isovaleric acid, propionic acid, or valeric acid among the
500 three diet groups (**Supplemental Table 8**).
501
502 **4. Discussion**

503 Elevated body fat impacts pancreatic cancer development and is an important modifiable
504 risk factor for its prevention (37). In this work, we characterized how weight normalization via
505 dietary switch would impact pancreatic carcinogenesis and the associated mechanisms. We
506 observed that mice fed a DIO exhibited a significant acceleration of markers associated with
507 pancreatic carcinogenesis, and that this was slowed down in mice that underwent a dietary
508 switch from DIO back to a CD. Mechanistically, the effect of the dietary switch appears to be
509 multifactorial, including the inhibition of ERK and STAT3 pathways in males, repression of
510 EpOME, and the modulation of the microbiota.

511 Reducing the risk of obesity-associated cancers with weight loss interventions is an active
512 area of research. Data collected in the post-bariatric surgery population suggests that the risk of
513 developing pancreatic cancer is significantly reduced following surgical weight loss (6, 11, 12).
514 A less invasive approach to weight management, the high-fat to a low-fat dietary switch, has
515 demonstrated positive effects when investigated in animal models of acute lymphoblastic
516 anemia, colon cancer, and endometrial cancer (16, 38, 39). In our study, the dietary switch-
517 induced weight led to a normalization of the mesenteric adipose depot size. This is salient
518 because visceral adipose depot leads to inflammatory changes that drive cancer (9, 40) and
519 abdominal adiposity is a more important causal risk factor for pancreatic cancer than obesity
520 (41). Interestingly, there was a significant positive correlation between fat mass and ADM, with
521 mice fed the DIO having higher fat mass and increased ADM percentage, highlighting the link
522 between adipose depots and carcinogenesis.

Diets high in fat promote pancreatic cancer development compared to diets low in fat, (42). We observed that male mice fed a DIO for the entire 21 weeks had higher pancreas weights, higher levels of ADM, increased cases with high-grade PanINs, and fibrosis when compared to the CD-fed mice. Similarly, we recently reported an increase in ADM, fibrosis, and proliferation in response to feeding a DIO for 8 weeks in KC mice (9, 10), which corresponds to the time when mice underwent the dietary switch. Importantly, switching the diet from a DIO to a CD slowed the carcinogenesis-promoting effects of DIO, lowering levels of fibrosis and ADM.

Interestingly, pancreatic cancer was identified only in the KC male mice fed the DIO throughout the 21-week feeding period, while no cancers were found in the CD and DIO→CD-fed mice. Of note, the induction of cancer in our study was milder than previously shown in the same KC mouse model. For example, in KC mice fed a high fat, high calorie (HFCD) diet, Chang et al. observed four cases of pancreatic cancer out of nine male mice and zero cases in female mice at 6 months of age (43). The composition of the HFCD was considerably different containing 40% energy from corn oil (very high in omega-6 fatty acids) and 34% energy from sucrose. It's possible that our low sucrose diet (5.5% kcal from sucrose) with different dietary fat quantity (60% energy from fat) and composition (higher in saturated and monounsaturated, with a 10:1 ratio of omega 6 to omega-3 fatty acids) contributed to some of the differences we observed.

Several mechanisms linking adiposity and pancreatic cancer development have been proposed. The RNAseq data strongly suggest that DIO's effect is led by a complex and multifactorial effect, including alterations in various genes involved in pancreatic secretions, inflammation, immune function, metabolism, and cancer-related pathways.

Pancreatic endocrine-exocrine signaling have been shown to regulate pancreatic carcinogenesis in the context of obesity (13). Our findings suggest that DIO increased the expression of multiple pancreatic secretion enzymes, including phospholipase C, protein kinase C beta, cystic fibrosis transmembrane conductance regulator and inositol 1,4,5-trisphosphate receptor 1. Of note, many of these have been associated with increased inflammation and

549 tumorigenesis (44-47). Specifically, phospholipase C plays a pivotal role regulating protein
550 kinases C and D, which can lead to ERK activation followed by cell proliferation, suggesting a
551 potential mechanism linking obesity to pancreatic carcinogenesis (48, 49). Remarkably, all of
552 these were normalized following dietary switch.

553 By affecting immune and metabolic functions and triggering inflammation, a high fat diet
554 can create an environment favorable for pancreatic cancer development and progression (50).
555 Interestingly, our data show that switching to a low-fat diet can counteract high fat diet-induced
556 genomic modulations and the activation of immune and inflammation-related genes. Importantly,
557 many of identified pathways could be modulated by key transcription factors including NF-κB,
558 and STAT3. The STAT3 pathway regulates angiogenesis, cell proliferation, immune escape, and
559 survival and is therefore a major player in the pancreatic cancer prevention and treatment
560 landscape (51). We recently showed that a DIO can increase STAT3 phosphorylation after only
561 8-weeks (10). After 21 weeks of treatment, DIO increased levels of STAT3 phosphorylation,
562 which returned to CD-fed levels following the dietary change from DIO to CD.

563 DIO also increased the activation of the RAF/MEK/ERK pathway, which is often
564 upregulated in pancreatic cancer and promotes cell growth, differentiation, and survival (52). Our
565 findings in male mice, are consistent with recent studies that demonstrate that DIO can impact
566 the ERK1/2 pathway even at early stages (9, 10). Critically, changing the diet resulted in a
567 reversal of phosphorylated ERK1/2 levels in male mice back to CD levels. Given that the changes
568 in ERK due to DIO (increase in males and no change in females) mirrored the changes in ADM,
569 this suggests that ERK is an important driver of carcinogenesis process associated with DIO, at
570 least in males.

571 A significant finding of our study was that the dietary switch reverted the increased
572 EpOMEs, which are epoxy metabolites of LA, induced by DIO. In particular, DIO increased the
573 concentrations of EpOMEs in the pancreas and these were normalized in the dietary switch
574 group. Previous research has shown that EpOMEs have an array of detrimental effects on

human health, including pulmonary edema, lung injury, and cardio-depression (53-55). In terms of cancer, previous studies by us and others have shown that EpOMEs induce inflammation and promote tumorigenesis. Indeed, we have shown that EpOME induced the production of pro-inflammatory cytokines in intestinal cells and colon cancer cells, and systematic administration of EpOME increased the development of colon cancer in mice (31, 56). 12,13-EpOME has been shown to promote the invasive and migratory abilities of cancer cells by regulating the epithelial-mesenchymal transition (EMT), a critical process in cancer metastasis (57). Moreover, EpOMEs facilitate breast cancer development though an NF-κB-dependent mechanism (58). Additionally, research indicates that EpOME can activate signaling pathways such as TLR4/AKT, further driving cancer progression (57). In addition, our data showed that DIO increased the expression of 5-LOX, a well-established pro-inflammatory enzyme (34), and elevated the concentrations of 5-LOX-derived eicosanoid metabolites such as 9-HODE. Thus, these findings suggest that increases in fatty acid metabolites, such as EpOMEs and 9-HODE, could represent a cellular mediator linking diet-induced obesity and pancreatic carcinogenesis.

The gut microbiota is increasingly recognized as a key mediator of PDAC progression (59), with various strategies to modulate the gut microbiome in PDAC currently under investigation (60). For instance, human fecal microbiota transplantation can influence PDAC tumor response by altering the gut microbiota and the immune system (61-63). DIO-fed KC mice showed the highest relative abundance of Firmicutes, aligning with studies that report an increased Firmicutes to Bacteroidota ratio in obese humans (64-66). Interestingly, the DIO→CD group exhibited an increase in Bacteroidota and a decrease in Firmicutes. This change is consistent with research indicating that weight loss results in similar phylum-level changes in humans (67). In relation to pancreatic cancer, studies have shown increased Bacteroides and decreased Firmicutes in the gut microbiome of PDAC patients, potentially due to detrimental late-stage cancer-related weight loss (36). Within the Firmicutes phylum, the genus *Dubosiella* was more abundant in CD-fed mice and lower in DIO-fed mice, suggesting a possible link to

pancreatic cancer precursors, as higher *Dubosiella* levels were observed in mice with diabetes (68).

Another interesting finding was that mice fed DIO presented with lower relative abundance of *Faecalibaculum.* Previous studies have highlighted the critical role of *Faecalibaculum*, in regulating tumor growth. Zagato et al. discovered that *Faecalibaculum rodentium* was significantly under-represented during the early stages of tumorigenesis in ApcMin/+ mice compared to wild-type mice, and it was found to inhibit intestinal tumor cell proliferation (69). Furthermore, *Faecalibaculum* has been shown to inhibit tumor growth in breast cancer models (70), and increase in response to ketogenic diet feeding and gemcitabine treatment in pancreatic cancer (71). This is consistent with our findings that DIO reduces *Faecalibaculum* levels while *Faecalibaculum* levels were restored to CD levels after switching from DIO to CD, which highlights the putative importance of this bacteria in regulating carcinogenesis.

Overall, these patterns suggest that obesity-induced microbiome alterations may influence pancreatic cancer progression. However, the microbiome is highly complex and changes in one microbe's abundance are unlikely to solely determine disease outcomes. Additional research is still needed to better understand the role of the microbiome in pancreatic cancer development.

It is likely that both high body fat and dietary fat intake drive pancreatic carcinogenesis and it is difficult to isolate these two variables within our study design. Although we observed a significant positive correlation between body weight gain and ADM, future studies investigating how high dietary fat intake promotes pancreatic cancer development in the absence of obesity may opt to feed the DIO diet in a calorie-controlled method (i.e. matching the calories consumed by the control group). In addition, we cannot rule out that the differences in vitamin per calorie content between the CD and DIO diets might have affected tumor growth outcomes, since the

uncontrolled proliferation of tumor cells, which relies on altered cellular metabolism, is regulated by vitamins. Additional studies with comparable vitamin per calorie content in the diets are warranted. Finally, future studies in the field of obesity and cancer would be strengthened by the inclusion of energy expenditure measurements to better determine the contributors to energy balance.

In summary, this study showed that feeding a DIO accelerates pancreatic carcinogenesis, and that a timely dietary change from a DIO to a CD, which normalizes body weight, can slow down these pro-cancer events. Considering the cancer-promoting effects of post-industrial era dietary patterns —high in total fat, saturated fat and omega-6 fatty acids, high in sugar, and low in fiber—changes in dietary fat quantity that lead to body weight normalization may represent a safe, cost-effective, and noninvasive approach to preventing pancreatic cancer. Mechanistically, these effects may be mediated by changes in global gene expression, gastrointestinal microbiome composition, and favorable alterations in the RAS/MAPK/ERK and STAT3 pathways in the pancreas.

Acknowledgements: Grant Support: Supported by funds from the University of California, Davis and NIFA-USDA (CA-D-NTR-2397-H) to GGM, grants from the Research Dietetic Practice Group and the Oncology Nutrition Dietetic Practice Group of the Academy of Nutrition and Dietetics to JW, and the Henry Jastro awards to JW and ASE. G.G.M acknowledges support from the Corinne L. Rustici Endowed Chair in Human Nutrition. This research was also supported by the Biorepository Shared Resources, funded by the UC Davis Comprehensive Cancer Center Support Grant awarded by the National Cancer Institute (NCI P30CA093373). The study sponsors had no role in the study design, in the collection, analysis, and interpretation of data; in the writing of the review manuscript; nor in the decision to submit the manuscript for publication. We would

like to acknowledge Dr. Michael L. Goodson for his technical expertise in diet manufacturing, and Jazmin Machuca for her assistance with animal data assessments.

Statement of Authors' Contributions: **J. Wirkus:** Investigation, project administration, data curation, formal analysis, visualization, funding acquisition, writing-original draft, writing-review and editing. **A.S. Ead:** Investigation, project administration, formal analysis, writing-review and editing. **I. Krga:** Investigation, formal bioinformatics analysis, writing-review and editing. **M.G.Pontifex, M Muller,' D Vauzour:** Microbiome analysis, editing and final content. **Y Wang, G Zhang:** Lipidomics analysis, writing-review, editing and final content. **K. Matsukuma:** Formal histological analysis, writing-review and editing. **G.G. Mackenzie:** Conceptualization, supervision, funding acquisition, validation, writing-original draft, project administration, writing-review, editing and final content.

All authors (JW, ASE, IK, YW, MP, MM, DV, KM, GZ, and GGM) have read and approved the final version. Study design in Figure 1A was created with BioRender.

References

1. Rahib L, Smith BD, Aizenberg R, Rosenzweig AB, Fleshman JM, Matrisian LM. Projecting cancer incidence and deaths to 2030: the unexpected burden of thyroid, liver, and pancreas cancers in the United States. Cancer Res. 2014 Jun 1;74:2913-21.
2. Siegel RL, Giaquinto AN, Jemal A. Cancer statistics, 2024. CA: a cancer journal for clinicians. 2024 Jan-Feb;74:12-49.
3. Stukalin I, Ahmed NS, Fundytus AM, Qian AS, Coward S, Kaplan GG, Hilsden RJ, Burak KW, Lee JK, et al. Trends and Projections in National United States Health Care Spending for Gastrointestinal Malignancies (1996-2030). Gastroenterology. 2022 Apr;162:1098-110 e2.
4. Eibl G, Rozengurt E. Obesity and Pancreatic Cancer: Insight into Mechanisms. Cancers (Basel). 2021 Oct 10;13.
5. Hopkins BD, Goncalves MD, Cantley LC. Obesity and Cancer Mechanisms: Cancer Metabolism. Journal of clinical oncology : official journal of the American Society of Clinical Oncology. 2016 Dec 10;34:4277-83.
6. Xu M, Jung X, Hines OJ, Eibl G, Chen Y. Obesity and Pancreatic Cancer: Overview of Epidemiology and Potential Prevention by Weight Loss. Pancreas. 2018 Feb;47:158-62.
7. Chang HH, Moro A, Takakura K, Su HY, Mo A, Nakanishi M, Waldron RT, French SW, Dawson DW, et al. Incidence of pancreatic cancer is dramatically increased by a high fat, high calorie diet in KrasG12D mice. PLoS One. 2017;12:e0184455.
8. Dawson DW, Hertzer K, Moro A, Donald G, Chang HH, Go VL, Pandol SJ, Lugea A, Gukovskaya AS, et al. High-fat, high-calorie diet promotes early pancreatic neoplasia in the conditional KrasG12D mouse model. Cancer Prev Res (Phila). 2013 Oct;6:1064-73.
9. Ead AS, Wirkus J, Matsukuma K, Mackenzie GG. A high-fat diet induces changes in mesenteric adipose tissue accelerating early-stage pancreatic carcinogenesis in mice. J Nutr Biochem. 2024 Sep;131:109690.
10. Machuca J, Wirkus J, Ead AS, Vahmani P, Matsukuma KE, Mackenzie GG, Oteiza PI. Dietary omega-3 Fatty Acids Mitigate Intestinal Barrier Integrity Alterations in Mice Fed a High-Fat Diet: Implications for Pancreatic Carcinogenesis. J Nutr. 2025 Jan;155:197-210.

11. Schauer DP, Feigelson HS, Koebnick C, Caan B, Weinmann S, Leonard AC, Powers JD, Yenumula PR, Arterburn DE. Bariatric Surgery and the Risk of Cancer in a Large Multisite Cohort. Annals of Surgery. 2019 Jan;269:95-101.

12. Fan H, Mao Q, Zhang W, Fang Q, Zou Q, Gong J. The Impact of Bariatric Surgery on Pancreatic Cancer Risk: a Systematic Review and Meta-Analysis. Obesity Surgery. 2023 2023/06/01;33:1889-99.

13. Chung KM, Singh J, Lawres L, Dorans KJ, Garcia C, Burkhardt DB, Robbins R, Bhutkar A, Cardone R, et al. Endocrine-Exocrine Signaling Drives Obesity-Associated Pancreatic Ductal Adenocarcinoma. Cell. 2020 May 14;181:832-47 e18.

14. Camp KK, Coleman MF, McFarlane TL, Doerstling SS, Khatib SA, Rezeli ET, Lewis AG, Pfeil AJ, Smith LA, et al. Calorie restriction outperforms bariatric surgery in a murine model of obesity and triple-negative breast cancer. JCI Insight. 2023 Sep 12;8.

15. Clontz AD, Gan E, Hursting SD, Bae-Jump VL. Effects of Weight Loss on Key Obesity-Related Biomarkers Linked to the Risk of Endometrial Cancer: A Systematic Review and Meta-Analysis. Cancers (Basel). 2024 Jun 11;16.

16. Bowers LW, Glenny EM, Punjala A, Lanman NA, Goldbaum A, Himbert C, Montgomery SA, Yang P, Roper J, et al. Weight Loss and/or Sulindac Mitigate Obesity-associated Transcriptome, Microbiome, and Protumor Effects in a Murine Model of Colon Cancer. Cancer Prev Res (Phila). 2022 Aug 1;15:481-95.

17. Salem AA, Mackenzie GG. Pancreatic cancer: A critical review of dietary risk. Nutr Res. 2018 Apr;52:1-13.

18. Hingorani SR, Petricoin EF, Maitra A, Rajapakse V, King C, Jacobetz MA, Ross S, Conrads TP, Veenstra TD, et al. Preinvasive and invasive ductal pancreatic cancer and its early detection in the mouse. Cancer Cell. 2003 Dec;4:437-50.

19. Hruban RH, Adsay NV, Albores-Saavedra J, Anver MR, Biankin AV, Boivin GP, Furth EE, Furukawa T, Klein A, et al. Pathology of genetically engineered mouse models of pancreatic exocrine cancer: consensus report and recommendations. Cancer Res. 2006 Jan 1;66:95-106.

20. Hingorani SR, Petricoin EF, III, Maitra A, Rajapakse V, King C, Jacobetz MA, Ross S, Conrads TP, Veenstra TD, et al. Preinvasive and invasive ductal pancreatic cancer and its early detection in the mouse. Cancer Cell. 2003;4:437-50.

21. Percie du Sert N, Hurst V, Ahluwalia A, Alam S, Avey MT, Baker M, Browne WJ, Clark A, Cuthill IC, et al. The ARRIVE guidelines 2.0: Updated guidelines for reporting animal research. BMC Veterinary Research. 2020 2020/07/14;16:242.

22. Nutrient Requirements of Laboratory Animals: Fourth Revised Edition, 1995. Washington (DC); 1995.
23. Mazur PK, Siveke JT. Genetically engineered mouse models of pancreatic cancer: unravelling tumour biology and progressing translational oncology. Gut. 2012 Oct;61:1488-500.
24. Basturk O, Hong SM, Wood LD, Adsay NV, Albores-Saavedra J, Biankin AV, Brosens LA, Fukushima N, Goggins M, et al. A Revised Classification System and Recommendations From the Baltimore Consensus Meeting for Neoplastic Precursor Lesions in the Pancreas. The American journal of surgical pathology. 2015 Dec;39:1730-41.
25. Bradford MM. A rapid and sensitive method for the quantitation of microgram quantities of protein utilizing the principle of protein-dye binding. Analytical Biochemistry. 1976 1976/05/07/;72:248-54.
26. Pang Z, Chong J, Zhou G, de Lima Morais DA, Chang L, Barrette M, Gauthier C, Jacques PE, Li S, Xia J. MetaboAnalyst 5.0: narrowing the gap between raw spectra and functional insights. Nucleic Acids Res. 2021 Jul 2;49:W388-W96.
27. Tang D, Chen M, Huang X, Zhang G, Zeng L, Zhang G, Wu S, Wang Y. SRplot: A free online platform for data visualization and graphing. PLoS One. 2023;18:e0294236.
28. Zhou Y, Zhou B, Pache L, Chang M, Khodabakhshi AH, Tanaseichuk O, Benner C, Chanda SK. Metascape provides a biologist-oriented resource for the analysis of systems-level datasets. Nature communications. 2019 Apr 3;10:1523.
29. Han H, Cho JW, Lee S, Yun A, Kim H, Bae D, Yang S, Kim CY, Lee M, et al. TRRUST v2: an expanded reference database of human and mouse transcriptional regulatory interactions. Nucleic Acids Res. 2018 Jan 4;46:D380-D6.
30. Davis AP, Grondin CJ, Johnson RJ, Sciaky D, Wiegers J, Wiegers TC, Mattingly CJ. Comparative Toxicogenomics Database (CTD): update 2021. Nucleic Acids Res. 2021 Jan 8;49:D1138-D43.
31. Wang W, Yang J, Edin ML, Wang Y, Luo Y, Wan D, Yang H, Song CQ, Xue W, et al. Targeted Metabolomics Identifies the Cytochrome P450 Monooxygenase Eicosanoid Pathway as a Novel Therapeutic Target of Colon Tumorigenesis. Cancer Res. 2019 Apr 15;79:1822-30.
32. Wang Q, Garrity George M, Tiedje James M, Cole James R. Naïve Bayesian Classifier for Rapid Assignment of rRNA Sequences into the New Bacterial Taxonomy. Applied and Environmental Microbiology. 2007 2007/08/15;73:5261-7.
33. Quast C, Pruesse E, Yilmaz P, Gerken J, Schweer T, Yarza P, Peplies J, Glöckner FO. The SILVA ribosomal RNA gene database project: improved data processing and web-based tools. Nucleic Acids Research. 2013;41:D590-D6.

34. Funk CD. Prostaglandins and leukotrienes: advances in eicosanoid biology. Science. 2001 Nov 30;294:1871-5.
35. Zhang G, Kodani S, Hammock BD. Stabilized epoxygenated fatty acids regulate inflammation, pain, angiogenesis and cancer. Prog Lipid Res. 2014 Jan;53:108-23.
36. Ren Z, Jiang J, Xie H, Li A, Lu H, Xu S, Zhou L, Zhang H, Cui G, et al. Gut microbial profile analysis by MiSeq sequencing of pancreatic carcinoma patients in China. Oncotarget. 2017 Nov 10;8:95176-91.
37. Wirkus J, Ead AS, Mackenzie GG. Impact of dietary fat composition and quantity in pancreatic carcinogenesis: Recent advances and controversies. Nutr Res. 2020 Dec 24;88:1-18.
38. Tucci J, Alhushki W, Chen T, Sheng X, Kim YM, Mittelman SD. Switch to low-fat diet improves outcome of acute lymphoblastic leukemia in obese mice. Cancer Metab. 2018;6:15.
39. Zhao Z, Wang J, Kong W, Fang Z, Coleman MF, Milne GL, Burkett WC, Newton MA, Lara O, et al. Intermittent energy restriction inhibits tumor growth and enhances paclitaxel response in a transgenic mouse model of endometrial cancer. Gynecologic oncology. 2024 Jul;186:126-36.
40. Himbert C, Delphan M, Scherer D, Bowers LW, Hursting S, Ulrich CM. Signals from the Adipose Microenvironment and the Obesity-Cancer Link-A Systematic Review. Cancer Prev Res (Phila). 2017 Sep;10:494-506.
41. Maina JG, Pascat V, Zudina L, Ulrich A, Pupko I, Bonnefond A, Balkhiyarova Z, Kaakinen M, Froguel P, Prokopenko I. Abdominal obesity is a more important causal risk factor for pancreatic cancer than overall obesity. European Journal of Human Genetics. 2023 2023/08/01;31:962-6.
42. Wirkus J, Ead AS, Mackenzie GG. Impact of dietary fat composition and quantity in pancreatic carcinogenesis: Recent advances and controversies. Nutrition Research. 2021 2021/04/01/;88:1-18.
43. Chang H-H, Moro A, Takakura K, Su H-Y, Mo A, Nakanishi M, Waldron RT, French SW, Dawson DW, Hines OJ. Incidence of pancreatic cancer is dramatically increased by a high fat, high calorie diet in KrasG12D mice. PloS one. 2017;12:e0184455.
44. McWilliams RR, Petersen GM, Rabe KG, Holtegaard LM, Lynch PJ, Bishop MD, Highsmith WE, Jr. Cystic fibrosis transmembrane conductance regulator (CFTR) gene mutations and risk for pancreatic adenocarcinoma. Cancer. 2010 Jan 1;116:203-9.

45. Ooi CY, Durie PR. Cystic fibrosis transmembrane conductance regulator (CFTR) gene mutations in pancreatitis. Journal of cystic fibrosis : official journal of the European Cystic Fibrosis Society. 2012 Sep;11:355-62.

46. Olive KP, Jacobetz MA, Davidson CJ, Gopinathan A, McIntyre D, Honess D, Madhu B, Goldgraben MA, Caldwell ME, et al. Inhibition of Hedgehog signaling enhances delivery of chemotherapy in a mouse model of pancreatic cancer. Science. 2009 Jun 12;324:1457-61.

47. Guha S, Lunn JA, Santiskulvong C, Rozengurt E. Neurotensin stimulates protein kinase C-dependent mitogenic signaling in human pancreatic carcinoma cell line PANC-1. Cancer Res. 2003 May 15;63:2379-87.

48. Sinnett-Smith J, Zhukova E, Hsieh N, Jiang X, Rozengurt E. Protein kinase D potentiates DNA synthesis induced by Gq-coupled receptors by increasing the duration of ERK signaling in swiss 3T3 cells. J Biol Chem. 2004 Apr 16;279:16883-93.

49. Rozengurt E. Protein kinase D signaling: multiple biological functions in health and disease. Physiology (Bethesda). 2011 Feb;26:23-33.

50. Greten FR, Grivennikov SI. Inflammation and Cancer: Triggers, Mechanisms, and Consequences. Immunity. 2019 Jul 16;51:27-41.

51. Corcoran RB, Contino G, Deshpande V, Tzatsos A, Conrad C, Benes CH, Levy DE, Settleman J, Engelman JA, Bardeesy N. STAT3 Plays a Critical Role in KRAS-Induced Pancreatic Tumorigenesis. Cancer Res. 2011 Jul 15;71:5020-9.

52. Adamopoulos C, Cave DD, Papavassiliou AG. Inhibition of the RAF/MEK/ERK Signaling Cascade in Pancreatic Cancer: Recent Advances and Future Perspectives. Int J Mol Sci. 2024 Jan 28;25.

53. Hu JN, Taki F, Sugiyama S, Asai J, Izawa Y, Satake T, Ozawa T. Neutrophil-derived epoxide, 9,10-epoxy-12-octadecenoate, induces pulmonary edema. Lung. 1988;166:327-37.

54. Fukushima A, Hayakawa M, Sugiyama S, Ajioka M, Ito T, Satake T, Ozawa T. Cardiovascular effects of leukotoxin (9, 10-epoxy-12-octadecenoate) and free fatty acids in dogs. Cardiovasc Res. 1988 Mar;22:213-8.

55. Ozawa T, Hayakawa M, Takamura T, Sugiyama S, Suzuki K, Iwata M, Taki F, Tomita T. Biosynthesis of leukotoxin, 9,10-epoxy-12 octadecenoate, by leukocytes in lung lavages of rat after exposure to hyperoxia. Biochem Biophys Res Commun. 1986 Feb 13;134:1071-8.

56. Zhang J, Yang J, Duval C, Edin ML, Williams A, Lei L, Tu M, Pourmand E, Song R, et al. CYP eicosanoid pathway mediates colon cancer-promoting effects of dietary linoleic acid. Faseb J. 2023 Jul;37:e23009.

57. Kong C, Yan X, Zhu Y, Zhu H, Luo Y, Liu P, Ferrandon S, Kalady MF, Gao R, et al. Fusobacterium Nucleatum Promotes the Development of Colorectal Cancer by Activating a Cytochrome P450/Epoxyoctadecenoic Acid Axis via TLR4/Keap1/NRF2 Signaling. Cancer Res. 2021 Sep 1;81:4485-98.

58. Ni KD, Fu X, Luo Y, He X, Yin HH, Mo DP, Wu JX, Wu MJ, Zheng X, et al. Epoxy metabolites of linoleic acid promote the development of breast cancer via orchestrating PLEC/NFkappaB1/CXCL9-mediated tumor growth and metastasis. Cell Death Dis. 2024 Dec 18;15:901.

59. Wei MY, Shi S, Liang C, Meng QC, Hua J, Zhang YY, Liu J, Zhang B, Xu J, Yu XJ. The microbiota and microbiome in pancreatic cancer: more influential than expected. Molecular cancer. 2019 May 20;18:97.

60. Chandra V, McAllister F. Therapeutic potential of microbial modulation in pancreatic cancer. Gut. 2021 Apr 27.

61. Riquelme E, Zhang Y, Zhang L, Montiel M, Zoltan M, Dong W, Quesada P, Sahin I, Chandra V, et al. Tumor Microbiome Diversity and Composition Influence Pancreatic Cancer Outcomes. Cell. 2019 Aug 8;178:795-806 e12.

62. Guo X, Wang P, Li Y, Chang Y, Wang X. Microbiomes in pancreatic cancer can be an accomplice or a weapon. Critical Reviews in Oncology/Hematology. 2024 2024/02/01/;194:104262.

63. Li JJ, Zhu M, Kashyap PC, Chia N, Tran NH, McWilliams RR, Bekaii-Saab TS, Ma WW. The role of microbiome in pancreatic cancer. Cancer and Metastasis Reviews. 2021 2021/09/01;40:777-89.

64. Turnbaugh PJ, Ley RE, Mahowald MA, Magrini V, Mardis ER, Gordon JI. An obesity-associated gut microbiome with increased capacity for energy harvest. Nature. 2006 2006/12/01;444:1027-31.

65. Ley RE, Turnbaugh PJ, Klein S, Gordon JI. Human gut microbes associated with obesity. Nature. 2006 2006/12/01;444:1022-3.

66. Turnbaugh PJ, Hamady M, Yatsunenko T, Cantarel BL, Duncan A, Ley RE, Sogin ML, Jones WJ, Roe BA, et al. A core gut microbiome in obese and lean twins. Nature. 2009 2009/01/01;457:480-4.

67. Li L, Li R, Tian Q, Luo Y, Li R, Lin X, Ou Y, Guo T, Chen X, et al. Effects of healthy low-carbohydrate diet and time-restricted eating on weight and gut microbiome in adults with overweight or obesity: Feeding RCT. Cell Reports Medicine. 2024;5.

68. Cao M, Peng Y, Lu Y, Zou Z, Chen J, Bottino R, Knoll M, Zhang H, Lin S, et al. Controls of Hyperglycemia Improves Dysregulated Microbiota in Diabetic Mice. Transplantation. 2021;105.

69. Zagato E, Pozzi C, Bertocchi A, Schioppa T, Saccheri F, Guglietta S, Fosso B, Melocchi L, Nizzoli G, et al. Endogenous murine microbiota member Faecalibaculum rodentium and its human homologue protect from intestinal tumour growth. Nat Microbiol. 2020 Mar;5:511-24.

70. McKee AM, Kirkup BM, Madgwick M, Fowler WJ, Price CA, Dreger SA, Ansorge R, Makin KA, Caim S, et al. Antibiotic-induced disturbances of the gut microbiota result in accelerated breast tumor growth. iScience. 2021 Sep 24;24:103012.

71. Cortez NE, Rodriguez Lanzi C, Hong BV, Xu J, Wang F, Chen S, Ramsey JJ, Pontifex MG, Müller M, Vauzour D. A ketogenic diet in combination with gemcitabine increases survival in pancreatic cancer KPC mice. Cancer research communications. 2022;2:951-65.

883

884

885 **Figure legends**

886

887 **Figure 1. The effects of switching from a high-fat diet to a low-fat diet on body weight and**
888 **body composition.** KC mice were fed for 21 week a control diet (CD), a high-fat diet-induced
889 obesity diet (DIO), or switched from a DIO to a CD at 3 months of age. **A-**Study design. **B-** Body
890 weight gain over the 21 wk feeding period in male and female mice. **C-** Body weight at 6 months
891 of age. **D-** Fat and lean tissue (%) at 3 months prior to diet switch. **E-** Body fat and lean tissue
892 percentage at 6 months of age. Data are shown as means ± SD of 8-12 animals/group/sex. (*p
893 < 0.05, ** p < 0.01, *** p < 0.001, one-way ANOVA).

894

895 **Figure 2. The effects of a diet switch on calorie intake and glycemic control.** KC mice were
896 fed for 21 week a control diet (CD), a high-fat diet-induced obesity diet (DIO), or switched from
897 a DIO to a CD at 3 months of age. **A-** Food intake (kcal/day) during the first 2 months of dietary
898 treatment. Data are shown as means ± SD. (*** p < 0.001, unpaired two-tailed t-test). **B:** Food
899 intake (kcal/day) during the last 3 months of dietary treatment. Data are shown as means ± SD
900 of 8-12 animals/group/sex. (*** p < 0.001, one-way ANOVA). **C-** Non-fasting capillary glucose
901 measured at endpoint in male and female mice. **D-** Hemoglobin A1c (HbA1c) measured at 6
902 months of age. Data are shown as means ± SD of n = 4-9 animals/group/sex. (* p < 0.05, one-
903 way ANOVA).

904

905 **Figure 3. The effects of normalizing body weight with a diet switch on pancreatic**
906 **carcinogenesis.** KC mice were fed for 21 week a control diet (CD), a high-fat diet-induced
907 obesity diet (DIO), or switched from a DIO to a CD at 3 months of age. **A-** Pancreas weight. **B-**
908 Representative H&E, and Masson's trichrome histology images of the pancreas (10x) are shown.

Data were quantified and results are shown as mean ± SD of 6-12 animals/group/sex. (*p < 0.05, ** p < 0.01, *** p < 0.001, one-way ANOVA). **C-** Correlation between acinar-to-ductal metaplasia and body weight. Linear regression showing the relationship between changes in body weight and acinar-to-ductal metaplasia (ADM) at the end of the study. Control diet (CD) are represented by white circles, a high-fat diet-induced obesity diet (DIO) are represented by the black circles, and a switched from a DIO to a CD group (DIO→CD) is represented by the grey circles. **D-** Table highlighting high-grade PanIN cases in male and female KC mice after 21 weeks on the diet. **E-** Table highlighting pancreatic cancer incidence cases in male and female KC mice after 21 weeks on the diet.

Figure 4. The effects of a high-fat diet (DIO) and a dietary switch to a low-fat diet (DIO→CD) on pancreatic gene expression. A. Volcano plot showing differentially expressed genes in the pancreas of DIO-fed mice relative to control diet (CD)-fed mice; **B.** Top significant pathways associated with DIO-modulated genes. Underlined pathways are those pathways enriched in DIO compared to CD. **C.** Volcano plot showing differentially expressed genes in the pancreas of mice that switched to CD compared to those that remained on DIO; **D.** Top significant pathways associated with genes modulated by the dietary switch Underlined pathways are those pathways enriched in DIO→CD group compared to DIO. In **A.** and **C.**, the x-axis represents log2 fold changes, and the y-axis represents -log10 (adjusted p-values), with red dots indicating upregulated genes and blue dots indicating downregulated genes. In **B.** and **D**., KEGG pathway enrichment analysis was used to identify significant pathways, arranged by -log10 adjusted p-value. The numbers above the bar charts indicate the number of differentially expressed genes within each pathway.

Figure 5. A dietary switch to a low-fat diet (DIO→CD) reverses changes in pancreatic gene expression induced by a high-fat (DIO). A. Principal component analysis (PCA) plot showing

the separation of pancreatic global gene expression profiles among the control diet (CD), DIO, and DIO→CD groups. Each dot represents an individual sample, and each color corresponds to a different group; **B**. Venn diagram of genes differentially modulated by DIO and DIO→CD, accompanied by a heatmap depicting expression profiles of 842 differentially expressed genes identified in both DIO/CD and DIO→CD/DIO across the three experimental groups. **C**. Pathways affected by both DIO and DIO→CD, arranged by function and adjusted p-value. The enrichment score indicates whether each pathway was depleted or enriched in the respective groups. **D, E-** Protein levels of p-STAT3 and p-ERK1/2 were measured in the pancreas by Western blot. Bands were quantified and values were referred to vinculin levels (loading control). Data are shown as mean ± SD of 5-6 animals/diet group/sex of 2-3 technical replicates (*p < 0.05, ** p < 0.01, one-way ANOVA).

Figure 6. The effects of normalizing body weight with a diet switch on lipids and their metabolites in the pancreas. KC mice were fed for 21 wk a control diet (CD), a high-fat diet-induced obesity diet (DIO), or switched from a DIO to a CD at 3 months of age. **A-**. Volcano plot showing differentially expressed metabolites in the pancreas of mice in the DIO versus CD and those that switched from DIO to CD compared to those that remained on DIO (p < 0.05, one-way ANOVA). **B, C**- Concentrations of select lipid metabolites in pancreatic tissue. Data are shown as mean ± SD of 7-8 animals/diet group (** p < 0.01, *** p < 0.001, **** p < 0.0001, one-way ANOVA).

Figure 7. The effects of normalizing body weight with a diet switch on gastrointestinal microbiome alpha and beta diversity. A- Shannon and Simpson indexes were determined in a control diet (CD), a high-fat diet-induced obesity diet (DIO), or switched from a DIO to a CD groups to evaluate the gut microbiota community diversity and richness among groups. Data were quantified and results are shown as mean ± SD of 6-8 animals/group. (*p < 0.05, one-way

961 ANOVA). **B-** Principal component analysis (PCA). PC1 (axis 1) and PC2 (axis 2) represent the
962 two most principal factors characterizing the bacterial profile among the 3 groups and their
963 contribution rates (%) are shown on the axes. **C-** Relative abundance of the top ten bacteria at
964 the phylum (*left*) and genus (*right*) level measured in fecal samples using 16s rRNA sequencing
965 among the 3 dietary treatment groups at the end of the feeding study.
966
967 **Figure 8. The effects of normalizing body weight with a diet switch on gastrointestinal**
968 **microbiome composition.**
969 **A-** LDA score computed from features differentially abundant among the CD, DIO and DIO→CD
970 groups. The criteria for feature selection is Log LDA Score > 4. **B-** Relative abundance of specific
971 microbes in the gastrointestinal microbiome. Levels of *Clostridia*, *Blautia*, *Oscilibacter*,
972 *Intestinimonas*, *Roseburia* and *Coledextribacter* among the 3 groups. Data are shown as mean
973 ± SD of 6-8 animals/diet group (*$p < 0.05$, Kruskal-Wallis test).
974
975

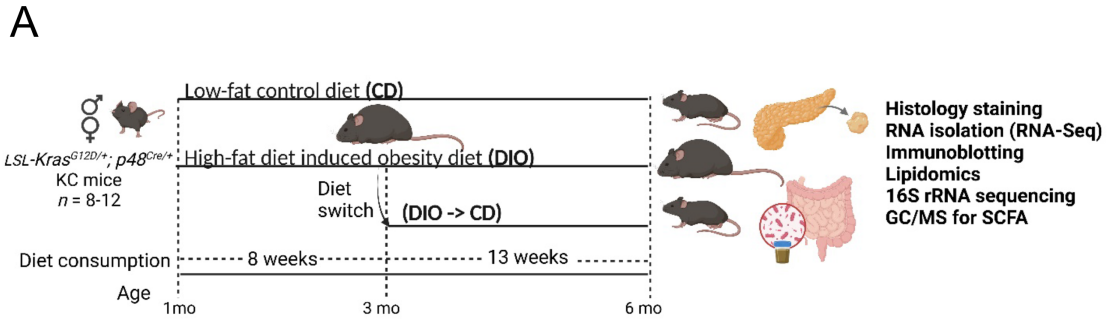

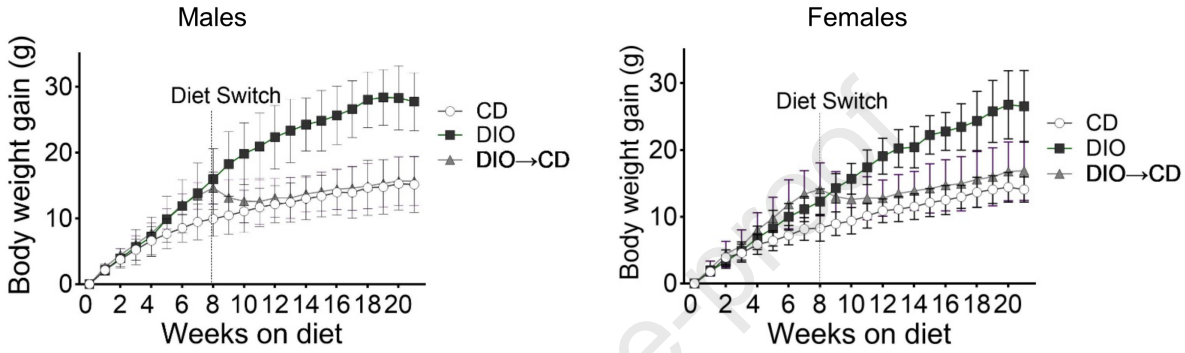

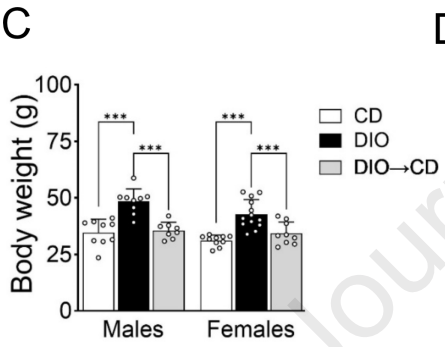

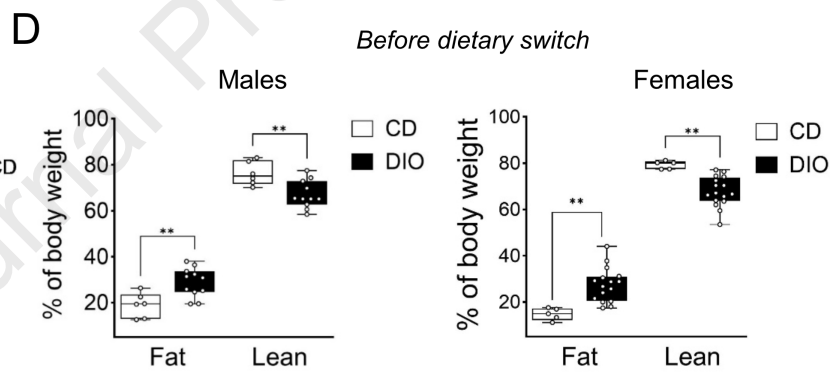

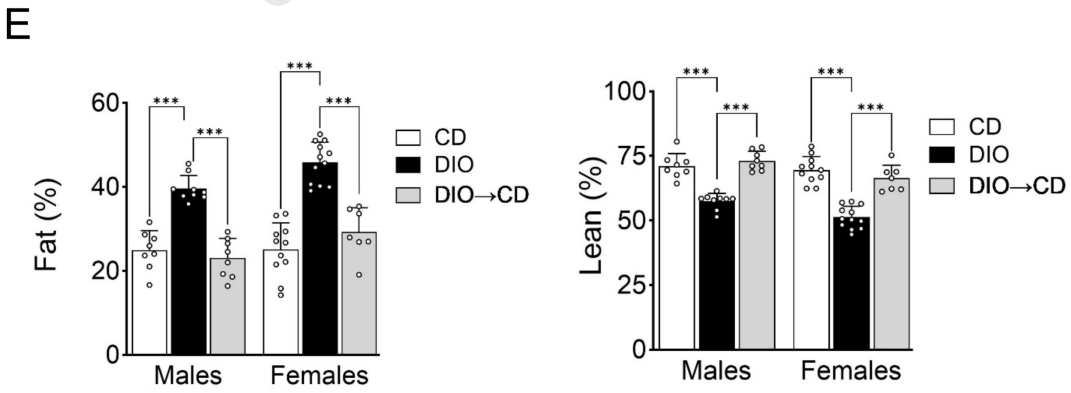

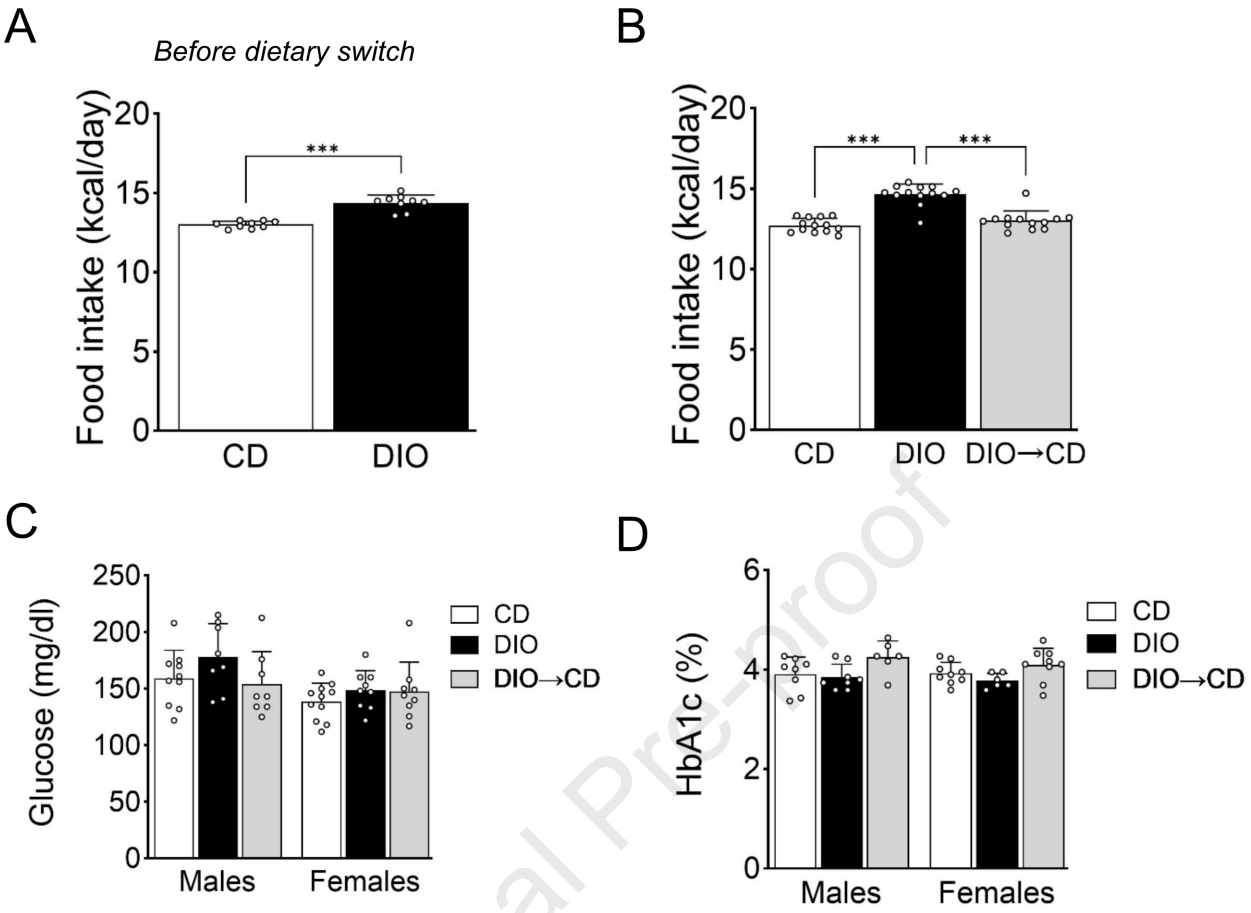

A

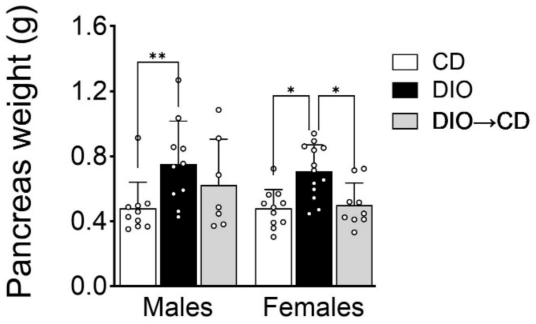

B

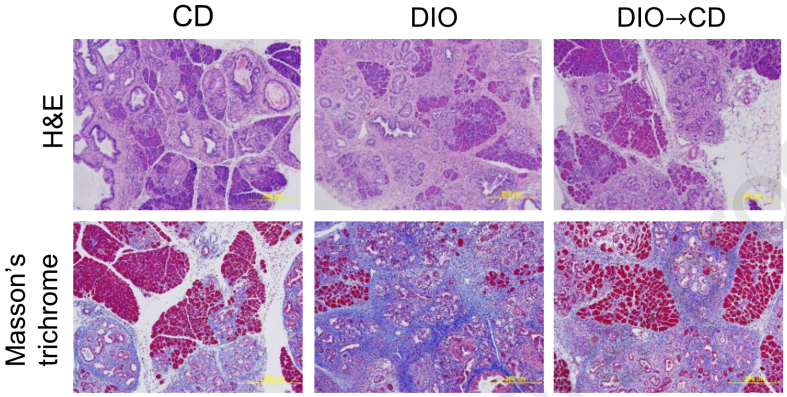

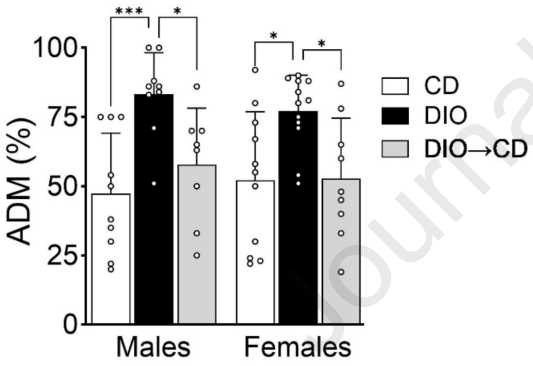

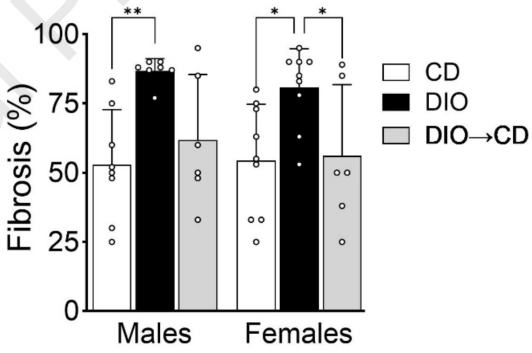

C

Diet group	All	Males	Females
CD	0/21 (0%)	0/10 (0%)	0/11 (0%)
DIO	2/21 (10%)	2/9 (22%)	0/12 (0%)
DIO→CD	0/17 (0%)	0/8 (0%)	0/9 (0%)

D

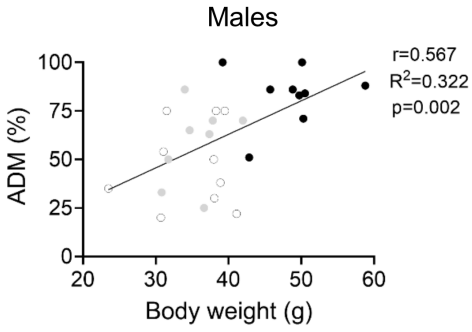

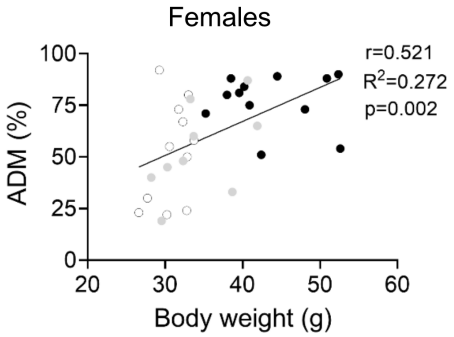

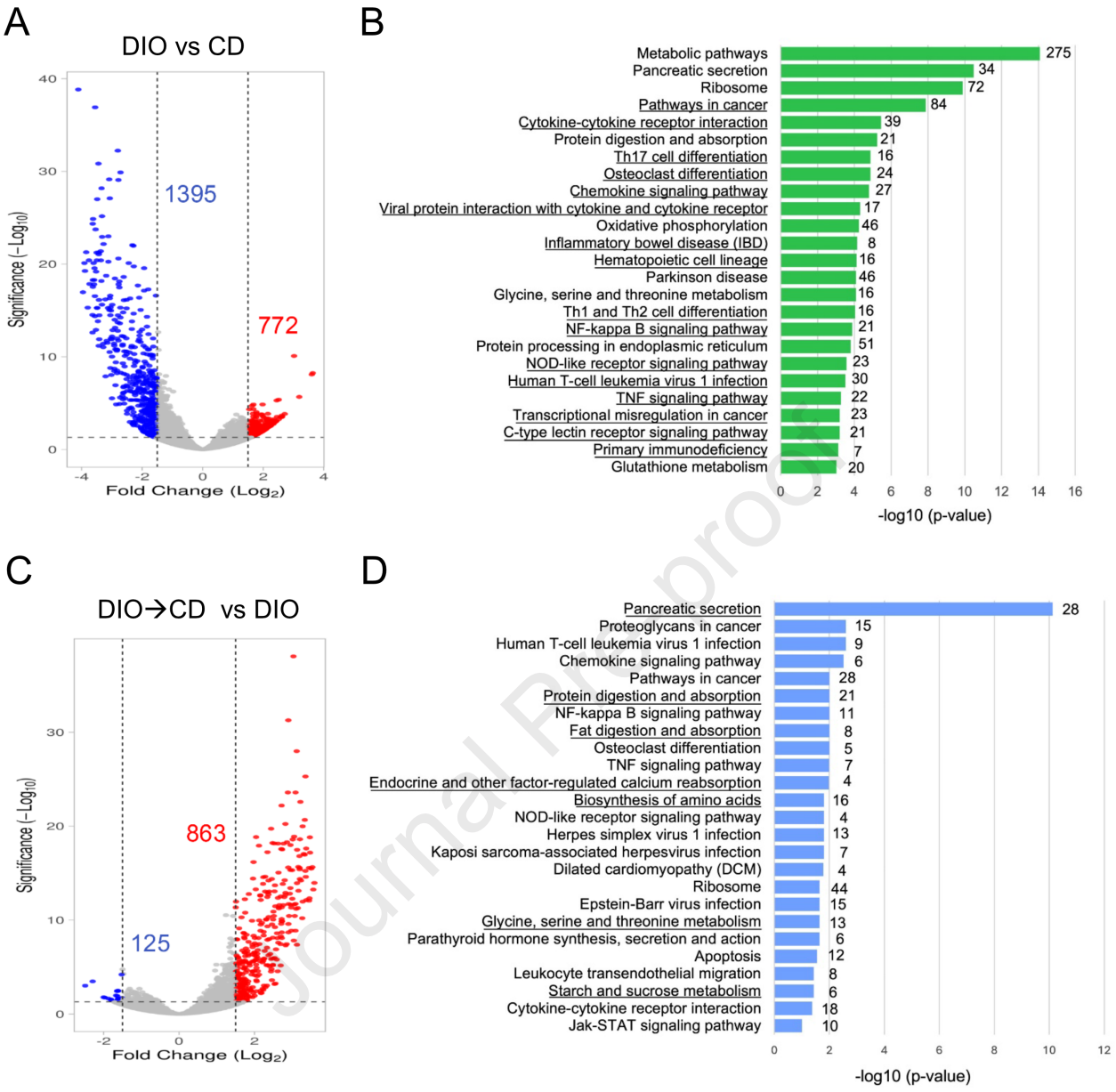

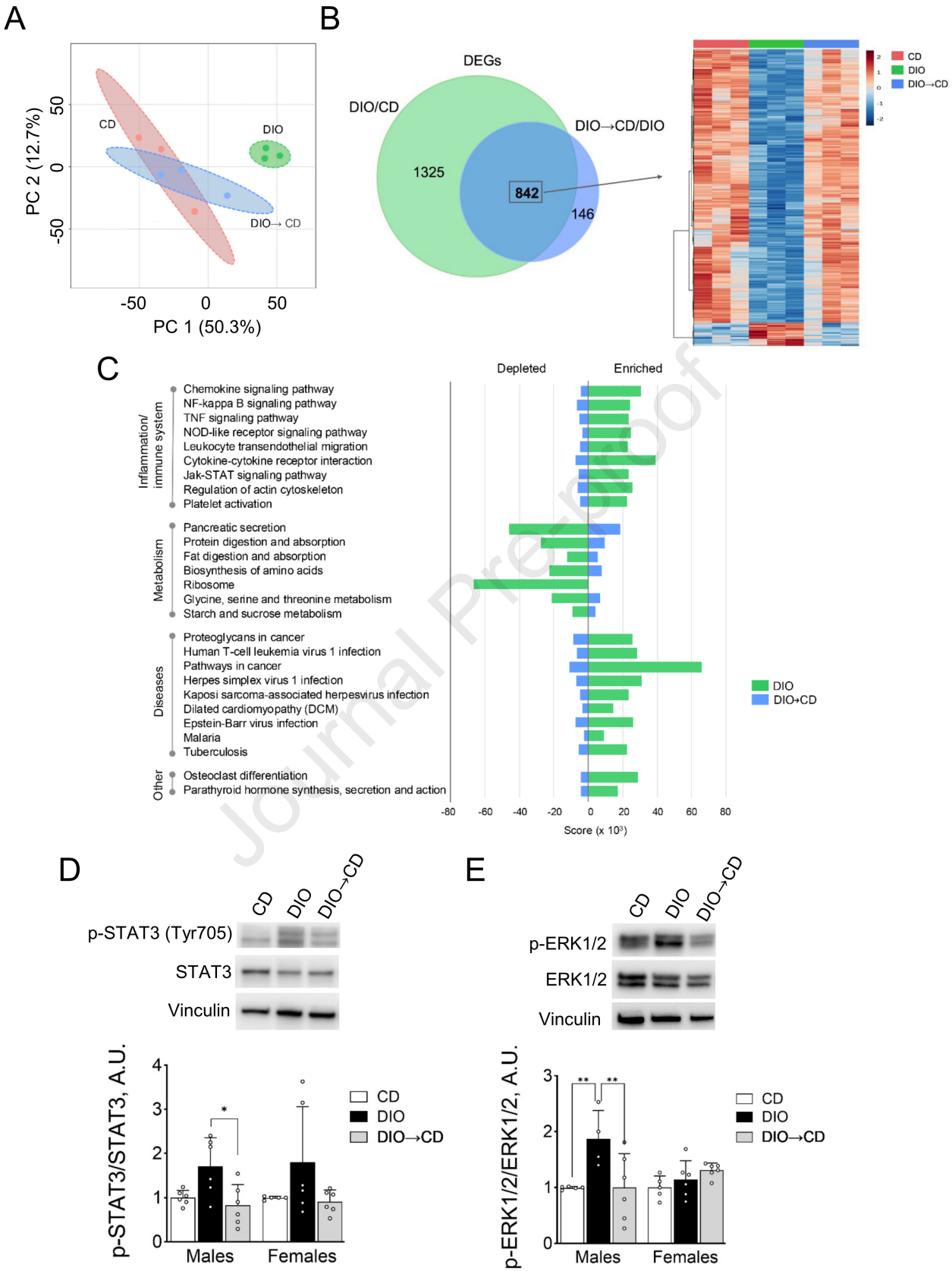
A
PC 2 (12.7%)
PC 1 (50.3%)
CD
DIO
DIO→ CD
B
DEGs
DIO/CD
DIO→CD/DIO
1325
842
146
CD
DIO
DIO→CD
C
Depleted
Enriched
Inflammation/ immune system
Chemokine signaling pathway
NF-kappa B signaling pathway
TNF signaling pathway
NOD-like receptor signaling pathway
Leukocyte transendothelial migration
Cytokine-cytokine receptor interaction
Jak-STAT signaling pathway
Regulation of actin cytoskeleton
Platelet activation
Metabolism
Pancreatic secretion
Protein digestion and absorption
Fat digestion and absorption
Biosynthesis of amino acids
Ribosome
Glycine, serine and threonine metabolism
Starch and sucrose metabolism
Diseases
Proteoglycans in cancer
Human T-cell leukemia virus 1 infection
Pathways in cancer
Herpes simplex virus 1 infection
Kaposi sarcoma-associated herpesvirus infection
Dilated cardiomyopathy (DCM)
Epstein-Barr virus infection
Malaria
Tuberculosis
Other
Osteoclast differentiation
Parathyroid hormone synthesis, secretion and action
DIO
DIO→CD
Score (x 10³)
D
CD
DIO
DIO→CD
p-STAT3 (Tyr705)
STAT3
Vinculin
p-STAT3/STAT3, A.U.
Males
Females
E
p-ERK1/2
ERK1/2
Vinculin
p-ERK1/2/ERK1/2, A.U.

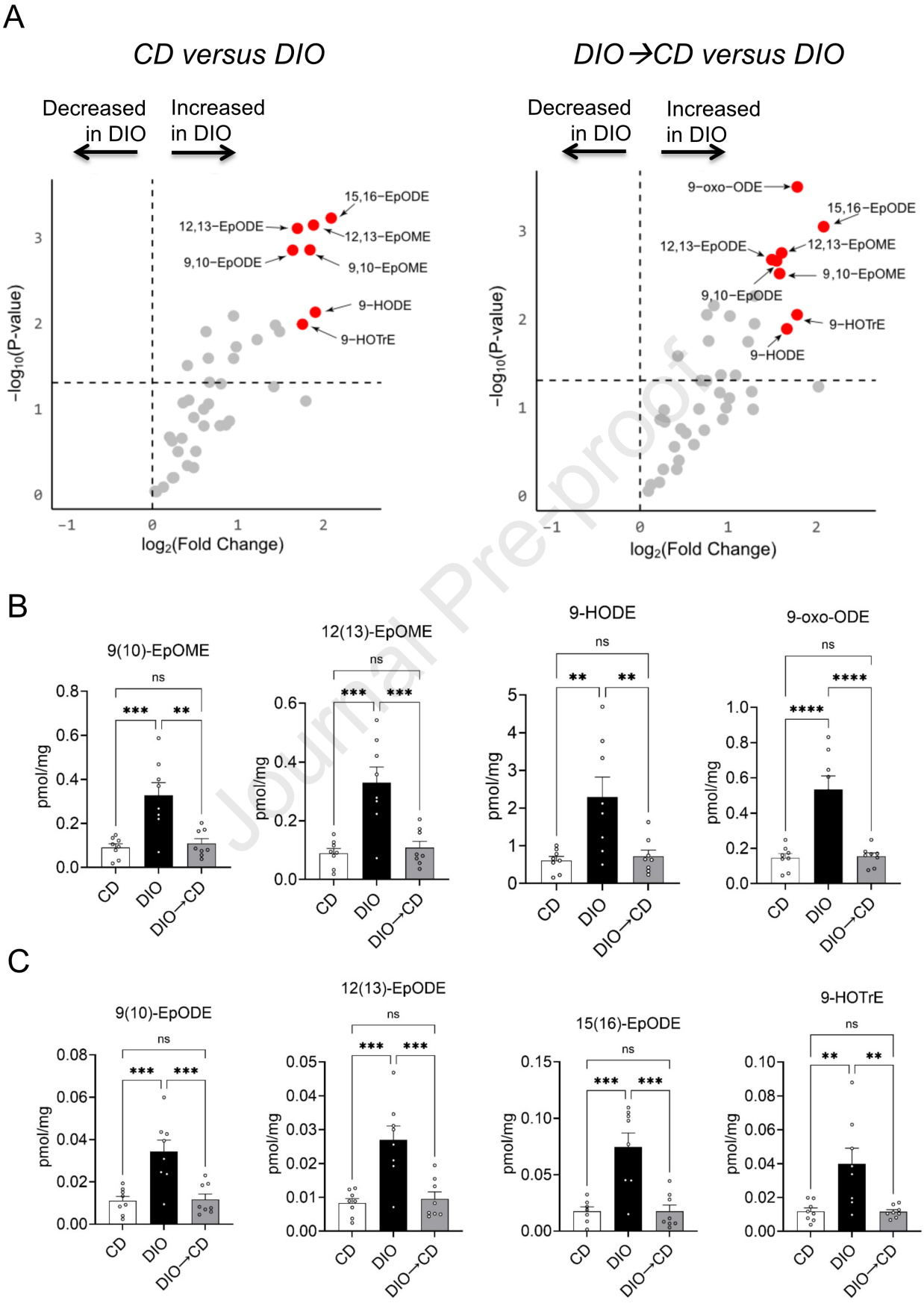

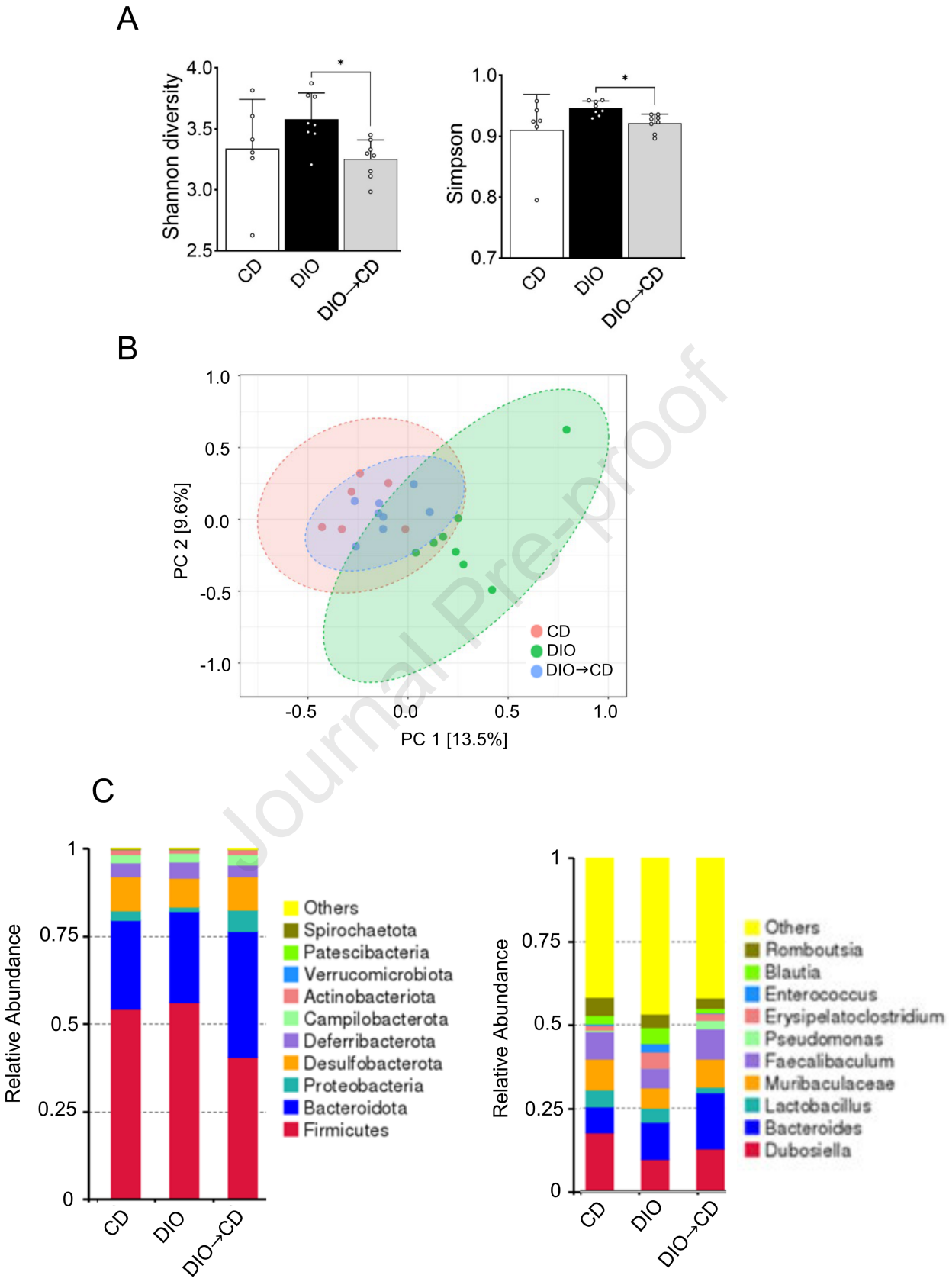

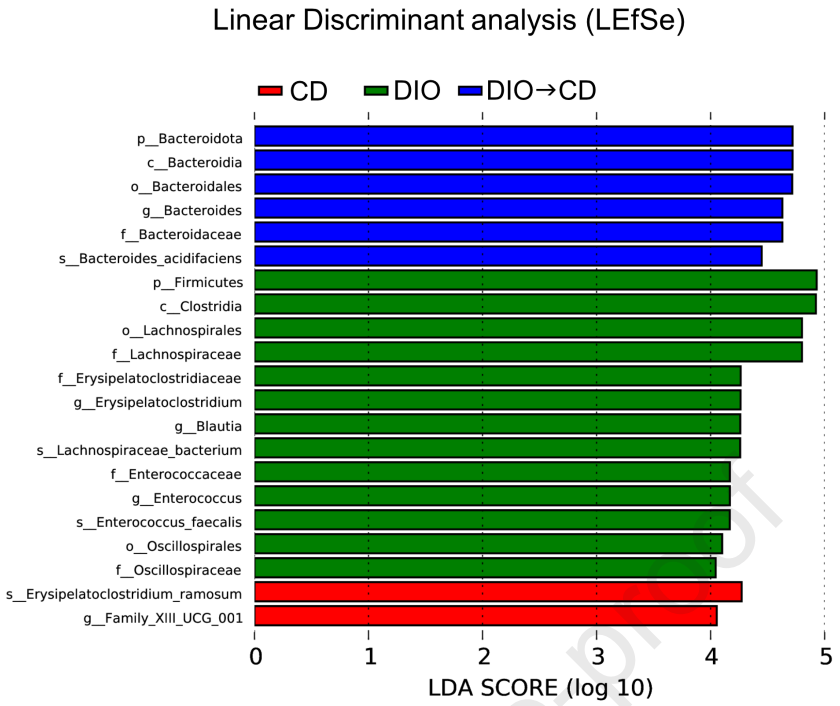

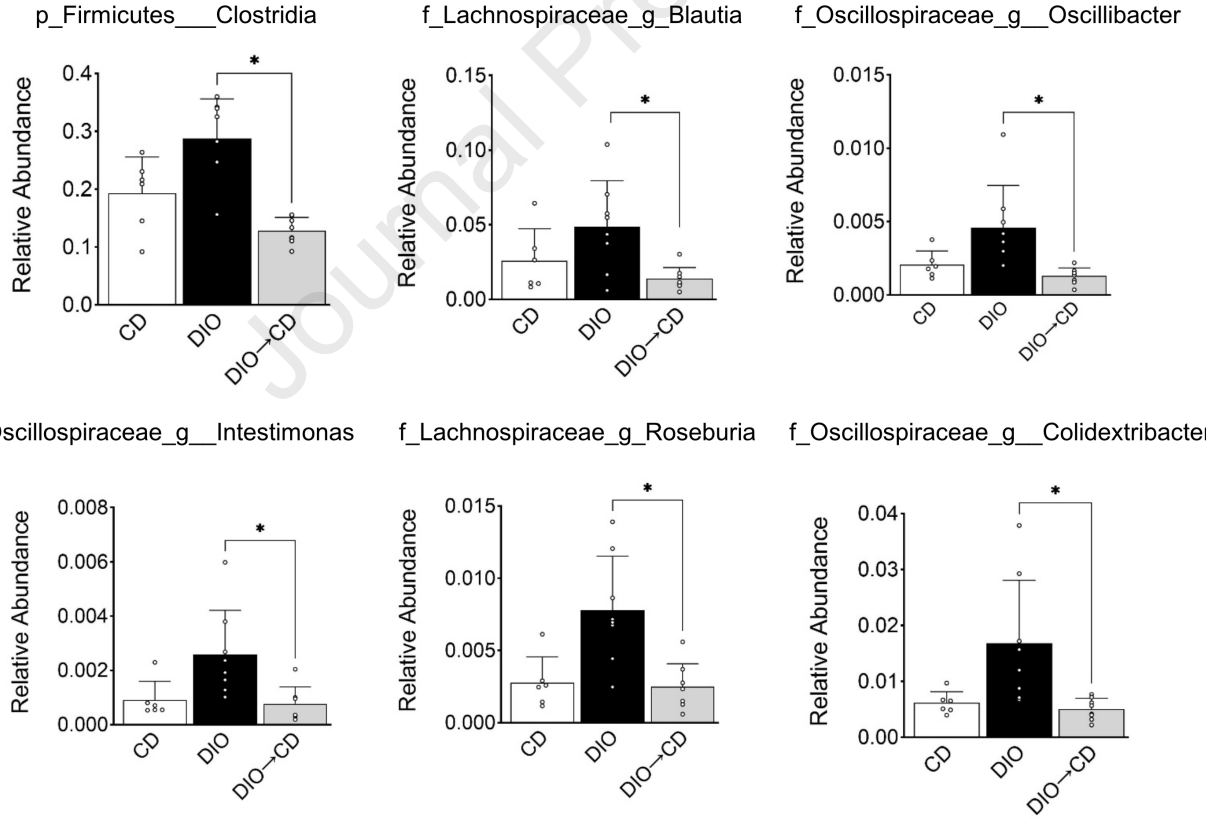

Declaration of interests

☐ The authors declare that they have no known competing financial interests or personal relationships that could have appeared to influence the work reported in this paper.

☒ The authors declare the following financial interests/personal relationships which may be considered as potential competing interests:

Gerardo G. Mackenzie reports financial support was provided by National Institutes of Health. Gerardo G. Mackenzie reports financial support was provided by National Institute of Food and Agriculture. If there are other authors, they declare that they have no known competing financial interests or personal relationships that could have appeared to influence the work reported in this paper.